Artificial Intelligence in Agriculture 9 (2023) 61–75

Contents lists available at ScienceDirect

Artificial Intelligence in Agriculture

journal homepage: http://www.keaipublishing.com/en/journals/artificial-intelligence-in-agriculture/

Development and evaluation of temperature-based deep learning models to estimate reference evapotranspiration

Amninder Singh *, Amir Haghverdi

Department of Environmental Sciences, University of California Riverside, Riverside, CA 92521, USA

ARTICLE INFO

Article history:
Received 19 January 2023
Received in revised form 5 August 2023
Accepted 13 August 2023
Available online 14 August 2023

Keywords:
CIMIS
Deep learning
Irrigation
Machine learning
Wavelet transform

ABSTRACT

Efficient irrigation management of urban landscapes is critical in arid/semi-arid environments and depends on the reliable estimation of reference evapotranspiration (ET_o). However, the available measured climatic data in urban areas are typically insufficient to use the standard Penman-Monteith for ET_o estimation. Therefore, smart landscape irrigation controllers often use temperature-based ET_o models for autonomous irrigation scheduling. This study focuses on developing deep learning temperature-based ET_o models and comparing their performance with widely used empirical temperature-based models, including FAO Blaney & Criddle (BC), and Hargreaves & Samani (HS). We also developed a simple free and easy-to-access tool called DeepET for ET_o estimation using the best-performing deep learning models developed in this study. Four artificial neural network (ANN) models were developed using raw weather data as inputs and the reconstructed signal obtained from the wavelet transform as inputs. In addition, long short-term memory (LSTM) recurrent neural network (NN) and one-dimensional convolution neural network (CNN) models were developed. A total of 101 active California Irrigation Management Information System (CIMIS) weather stations were selected for this study, with >725,000 data points expanding from 1985 to 2019. The performance of the models was evaluated against the standard CIMIS ET_o. When evaluated at the independent sites, the temperature-based DL (Deep Learning) models showed 15–20% lower mean absolute error values than the calibrated HS model. No improvement in the performance of the ANN models was observed using reconstructed signals obtained from the wavelet transform. Our study suggests that DL models offer a promising alternative for more accurate estimations of ET_o in urban areas using only temperature as input. The DeepET can be accessed from the Haghverdi Water Management Group website: http://www. ucrwater.com/software-and-tools.html.

1. Introduction

The FAO-56 Penman-Monteith is the accepted standardized method to estimate the reference evapotranspiration, ET_o (Allen et al., 2005). It accounts for both energy and mass transfer processes to provide a reliable estimation of ET_o. However, it requires a wide range of accurate meteorological data such as air temperature, humidity, solar radiation, and wind speed. Therefore, its implementation in data scarce situations, such as landscape irrigation management in urban areas, is challenging and limited. Promising results and significant water savings have been reported for landscape irrigation using smart evapotranspiration-based controllers with on-site weather sensors (Cardenas et al., 2021; Serena et al., 2020). These irrigation products often employ temperature-based ET_o equations in their scheduling algorithms due to the high cost of installing and maintaining a complete weather station (Davis and Dukes, 2010). Furthermore, for smart controllers that rely on interpolated ET_o for irrigation scheduling, air temperature data is widely available and spatially interpolated more accurately than other weather parameters (Temesgen et al., 2005).

Various studies have evaluated temperature-based ET_o models (Djaman et al., 2015; Hope and Evans, 1993; Liu et al., 2017;

Abbreviations: ET_o, Reference Evapotranspiration; BC, FAO-24 Blaney and Criddle model; HS, Hargreaves and Samani model; T_{min}, T_{max}, T_{av}, Daily minimum, maximum, and average temperature, respectively.; RH, Relative Humidity; U, Wind Speed; R_s, Global solar radiation; R_a, Extraterrestrial solar radiation; ML, Machine Learning; DL, Deep learning; WA, Wavelet analysis; ANN, Artificial neural network; ANN_all, Artificial neural network model with T_{min}, T_{max}, T_{av}, R_a, RH, and U as inputs.; ANN_T, Artificial neural network model with T_{min}, T_{max}, T_{av}, and R_a as inputs.; WA-ANN_all, Artificial neural network model with inputs (T_{min}, T_{max}, T_{av}, R_a, RH, and U) preprocessed using wavelet analysis.; WA-ANN_T, Artificial neural network model with inputs (T_{min}, T_{max}, T_{av}, and R_a) preprocessed using wavelet analysis.; LSTM, Long Short-Term Memory Recurrent Neural Network; CNN, Convolutional neural network; CIMIS, California Irrigation Management Information System.

* Corresponding author.
E-mail address: asing075@ucr.edu (A. Singh).

https://doi.org/10.1016/j.aiia.2023.08.003

Muhammad et al., 2019; Muniandy et al., 2016; Tabari et al., 2013; Xu and Singh, 2001). In California, data from CIMIS (California Irrigation Management Information System) stations have been widely used to evaluate the suitability of empirical temperature-based ET_o equations (Hargreaves and Allen, 2003; Hope and Evans, 1993; Temesgen et al., 2005). Recent multiyear turfgrass field irrigation research trials in Southern and Central California revealed accurate estimation of ET_o by the Weathermatic SL4800 smart irrigation controller using the Hargreaves and Samani equation (Hargreaves and Samani, 1985) compared to CIMIS ET_o (Haghverdi et al., 2021a, 2021b). However, the performance of ET_o estimation methods varies with climate and data availability (Djaman et al., 2015), and data requirements vary among models. Therefore, it is vital to evaluate temperature-based ET_o measurement methods and develop regional/site-specific calibration equations, which can help users determine the best approach depending on the availability of data and climate conditions (Kukal et al., 2020; Long et al., 2013).

Machine learning methods have also been proposed to estimate ET_o based on temperature and solar radiation data (Fan et al., 2018; Kisi and Alizamir, 2018). Algorithms such as artificial neural networks (ANN) and a combination of wavelet analysis/transform (WA) with ANN, referred to as WA-ANNs, have been explored in various hydrological studies (Adamala, 2018; Adamowski and Sun, 2010; Chen et al., 2020; Evrendilek, 2014; Falamarzi et al., 2014; Kisi and Alizamir, 2018; Partal, 2009; Traore et al., 2016, 2010). The WA-ANN was introduced by (Zhang and Benveniste, 1992) as an alternative approach to feedforward ANNs to denoise input data. Wavelets can also substitute for activation functions in feedforward ANNs, referred to as WNNs (Alexandridis and Zapranis, 2013). More recently, deep learning (DL) methods have been used for time series predictions (Han et al., 2021) and have shown better performance compared to other ML methods. Saggi and Jain (2019) found a superior estimation of ET_o with a deep feedforward ANN compared to other models such as the gradient boosting machine, the generalized linear model, and the random forest. In a study done in the Northeast plain of China, DL models such as temporal convolution neural network (CNN) and long short-term memory (LSTM) NN were found to outperform other temperature-based empirical models (Chen et al., 2020). The use of one-dimensional CNN models (1D CNN) for sequential or time-series data, such as ET_o, has demonstrated improved performance (Ferreira and da Cunha, 2020). Among these methods, hybrid CNN and LSTM models have also been used for ET_o estimation (Sharma et al., 2022; Yin et al., 2020).

CIMIS data have been used in multiple studies for ET_o estimations using ANN, WA-based, and DL models (Cobaner, 2013; Kişi, 2010; Partal, 2009; Sowmya et al., 2020). However, models are typically developed using ET_o data obtained from a limited number of sites and tested on the same sites. For instance, Long et al. (2022) recently demonstrated the applicability of the ANN and LSTM models for ET_o estimation using data from two weather stations in China and suggested that these models should be explored over more sites with varying climate conditions. Thus, a more extensive analysis of such methods is needed to evaluate the ability to produce generalized results over large regions. Furthermore, with some exceptions, little work has been reported on the use of LSTM and CNN for ET_o estimation. A particular focus on temperature-based models is required to assess their utility in urban irrigation management.

The main objectives of this study are (I) to evaluate the performance of two temperature-based empirical ET_o models, (II) to develop calibration equations for the empirical temperature-based models for all climate divisions in CA, (III) to develop and evaluate the accuracy of deep learning approaches (ANN, WA-ANN, LSTM, and 1D CNN) for ET_o estimations using different sets of input data, and (IV) validation of the empirical and DL ET_o models developed in this study.

2. Material and methods

2.1. Study region and data sources

This study was carried out in California using data obtained from automated CIMIS weather stations managed by the California Department of Water Resources (https://cimis.water.ca.gov/). In general, ET_o rates peak during the summer months and are low during winter under the Mediterranean climate of California, while precipitation is restricted primarily to winter and spring. Annual normal (1991–2020) minimum, maximum, and average temperatures vary from −6.8 to 18 °C, 2.5 to 32.8 °C, and − 1.75 to 24.7 °C, respectively. Statewide annual precipitation is about 56 cm. A total of 101 active CIMIS stations with available data ranging from 1985 to 2019 were selected. Approximately 50% of the stations had 25 to 35 years of data, and the remaining stations had at least ten years of data to ensure that a wide range of weather conditions and drought events were considered. Fig. 1 shows the locations of the selected CIMIS stations within the California aridity index map. The distribution of the weather parameters across the selected weather stations is shown in Fig. 2. Data quality was checked before modeling, and recordings with missing data were removed, and wind speed was limited between 0 and 20 m s^{-1}.

The aridity index, which can quantify precipitation availability over atmospheric water demand, was created following the classification recommended by the United Nations Environmental Programme (UNEP) and using the CGIAR-CSI Global-Aridity Database (Trabucco and Zomer, 2018). Most of the selected CIMIS stations belonged to the arid ($n = 48$) and semi-arid ($n = 39$) classes, while 4, 9, and 1 CIMIS stations belonged to hyper-arid, dry sub-humid, and humid classes, respectively. The spatial dataset of the seven climate divisions of California was obtained from the National Climatic Data Center- National Oceanic and Atmospheric Administration (NCDC-NOAA). The climate division data were used to perform a region-specific performance assessment of the models evaluated in this study.

2.2. Temperature-based empirical ET_o models

The following is a summary of the temperature-based empirical models used in this study. We used Python programming language version 3.8 (http://www.python.org) to calculate ET_o for all selected CIMIS stations. Furthermore, linear calibration equations were developed for the two regression-based models using the daily ET_o data for each climate division.

The FAO 24 – Blaney and Criddle method, BC (Allen and Pruitt, 1991; Donald Frevert et al., 1983; Doorenbos and Pruitt, 1977) is a modified version of the BC equation that includes correction factors to adjust for local weather or climatic conditions.

$$ET_o = A + B[p(0.46T_a + 8.13)] \tag{1}$$

$$A = 0.0043RHmin - \frac{n}{N} - 1.41 \tag{2}$$

$$B = 0.82 - 0.0041(RHmin) + 1.07\left(\frac{n}{N}\right) + 0.066(Ud) - 0.006(RHmin)\left(\frac{n}{N}\right) - 0.0006(RHmin)(Ud) \tag{3}$$

where $RHmin$ is the daily minimum relative humidity, Ud is the daytime wind speed measured at height 2 m, and n/N is the mean ratio of actual to possible sunshine hours that can be obtained from solar radiation estimates as:

$$\frac{n}{N} = 2\left(\frac{R_S}{R_a}\right) - 0.5 \tag{4}$$

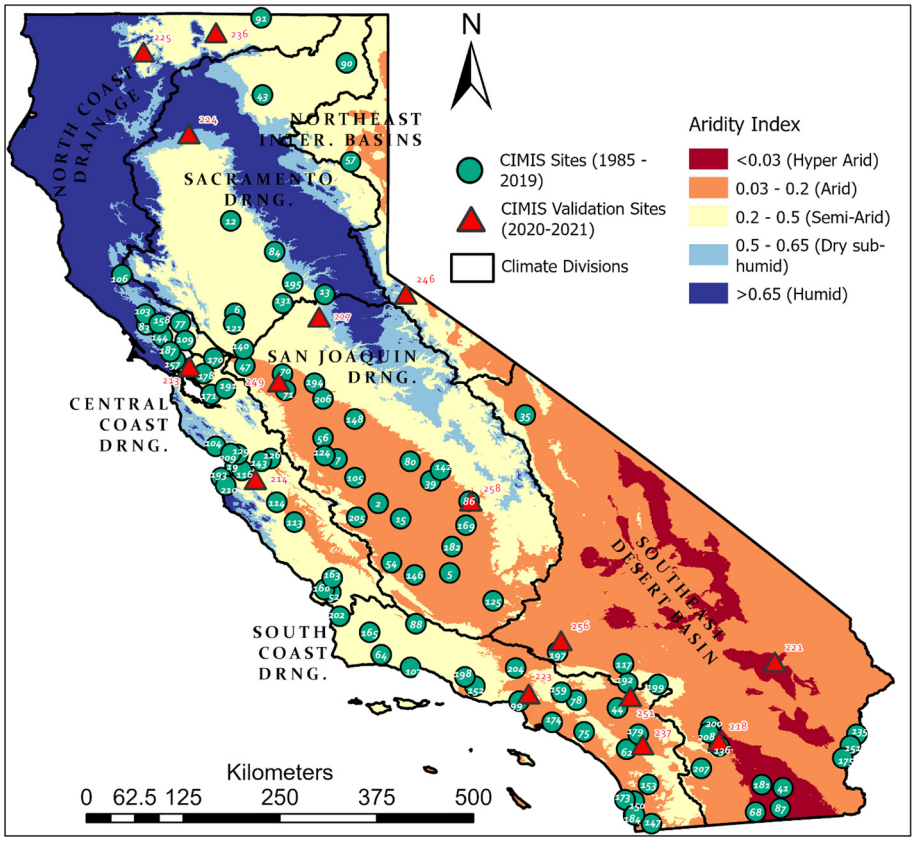

Fig. 1. Distribution of the CIMIS stations evaluated in this study across the state of California. The aridity index values were obtained from the CGIAR-CSI Global-Aridity Database, and the classes were mapped based on the United Nations Environmental Programme (UNEP) recommendations.

where R_a is the extraterrestrial radiation expressed in equivalent evaporation units [mm d^{-1}] and R_s is the global solar radiation at the surface [mm d^{-1}]. Extraterrestrial solar radiation (R_a) was calculated following the equations given by Allen et al. (1998), using the python library 'pyETo' (https://pyeto.readthedocs.io/en/latest/index.html). Daytime wind speed (*Ud*) was obtained by multiplying the 24-h measurements of wind speed by 1.3 (Doorenbos and Pruitt, 1977).

The Hargreaves and Samani method, HS (Hargreaves and Samani, 1985), uses air temperature and estimated extraterrestrial solar radiation for a given latitude and day to estimate ET_o.

$$ET_o = 0.0023R_a(T_a{}^\circ C + 17.8)\sqrt{T_{max} - T_{min}} \quad (5)$$

where $T_{max} - T_{min}$ is the difference between the daily maximum and minimum air temperatures [°C].

2.3. Deep learning models

In real-world applications, when all the necessary input variables are available, the application of FAO-56 Penman-Monteith as the standard physically based model is suggested for estimating ET_o. Therefore, the main focus of this study was to develop and evaluate temperature-based deep learning ET_o models. However, DL models with extra input variables, including relative humidity (RH) and wind speed (U) were developed to compare the maximum achievable performance of each DL approach.

2.3.1. Artificial neural network (ANN) models

Two feedforward backpropagation ANN models were developed with different combinations of input variables (Fig. 3). One model used several inputs, including T_{min}, T_{max}, T_a, RH, U, and R_a, while the other model only had T_{min}, T_{max}, T_a, and R_a as inputs. A total of 725,849 data points from 101 CIMIS stations were divided into five folds such that four folds were used for training and the remaining group (~20% of data) for testing the models. In addition, 12.5% of the training set was used as cross-validation for training of the DL models, helping to terminate the training and avoid overfitting. The maximum epoch (i.e., one cycle of a complete presentation of the training data set through the learning process) was set to 1000; however, early-stopping was implemented when the loss function did not improve for 20 consecutive epochs. By early-stopping the training of the model, the complexity of the model can be controlled, improving generalization (Yao et al., 2007). The model development process was repeated five times to ensure that data from all CIMIS stations had been in the test set. This approach assessed the generalizability of the models, as data from the same CIMIS station were never used in the training and test set simultaneously. The 'adam' optimizer function (Kingma and Ba, 2015) was used to train the feedforward ANN models, and the best weights and biases were automatically loaded for testing. The activation functions were 'ReLu' and 'linear' for the hidden and output layers, respectively. The Python library TensorFlow (TensorFlow Developers, 2021) was utilized to develop the ANN models.

The same steps as aforementioned were followed to develop WA-ANN models using the reconstructed signals obtained from the wavelet transform. Discrete wavelet transform (DWT) was applied to decompose the climatic time series of input predictors by passing through a series of high-pass and low-pass filters, separated at different scales. The Daubechies (db10) family of wavelets with decomposition a level of 10 (2–4–8–16–32–64–128–256–512–1024) was used. The original time series were decomposed into series of approximation(A) and detail(D) subseries. The correlation coefficient was computed between the ET_o data series and the decomposed subseries. The subseries with

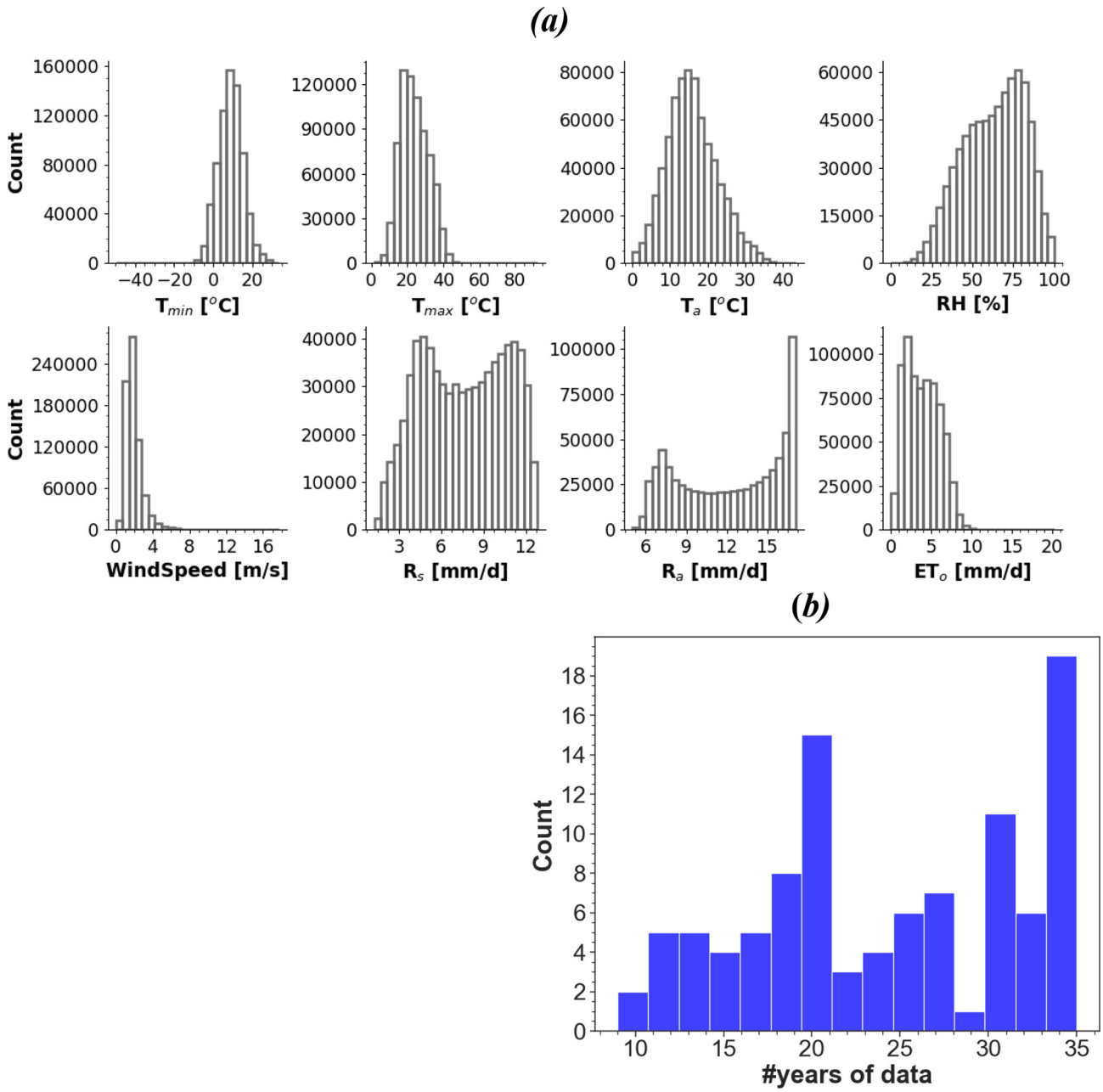

Fig. 2. Histograms of the meteorological variables (a) and availability of the data across CIMIS stations used in this study (b).

correlation coefficient values greater than ±0.1 were recognized as effective (Partal, 2009). The effective wavelet subseries were used to reconstruct the time series used as inputs to the ANN model. The Python library Pywavelets (Lee et al., 2019) was used for this analysis.

2.3.2. Long short-term memory (LSTM) and convolutional neural network (1D CNN) models

Long short-term memory (LSTM) layers are a type of recurrent unit often used in deep learning algorithms. The memory element present in its structure enables it to detect long-term dependencies of sequential tasks (Hochreiter and Schmidhuber, 1997), resulting in improved performance when dealing with time-series problems. Since the output of an LSTM unit at time step t is a function of all the inputs from the previous time step, it could be said that it has a form of *memory*. The LSTM unit preserves an internal state (long and short-term) across time steps and produces an output.

An LSTM unit consists of three gates that serve as controllers, as shown in Fig. 4(a):

- Forget Gate (f_t) - controls which parts of the long-term state should be forgotten.
- Input Gate (i_t)- Controls which parts of the $g(t)$ should be added to the long-term state.
- Output Gate (o_t) - controls if/when the remembered value is allowed to pass from the unit.

In Fig. 4(a), '*' and '+' are the element-wise multiplication and addition, respectively. Activation functions are sigmoid and hyperbolic tangent (tanh), and $g(t)$ represents candidate context value. The $\hat{y}$ values are the output from the unit; the x values are the input to the unit, and c values are the context values. The output and context values always feed their output to the next time step, and the context values allow the network to maintain the state between units.

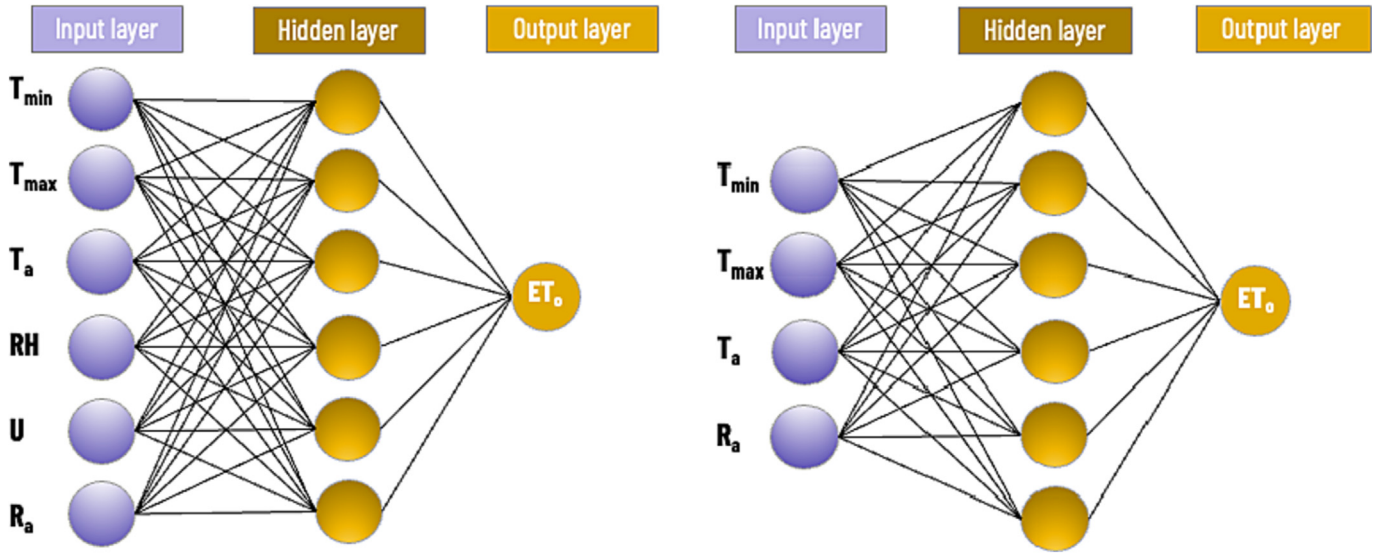

Fig. 3. The architecture of the feed-forward backpropagation neural network models that were developed in this study. T_{min}, T_{max}, and T_a are the daily minimum, maximum, and mean air temperature [°C], respectively; RH: Relative Humidity [%]; U: daily mean windspeed [m s^{-1}]; R_a: extraterrestrial solar radiation [mm d^{-1}].

In short, an LSTM cell can learn to recognize a vital input (input gate), store it in the long-term state, preserve it as long as it is needed (forget gate), and extract it whenever necessary. The LSTM NN architecture used in this study consisted of the input layer, a hidden layer with 48 LSTM units, another dense hidden layer with 24 units and ReLU activation function, followed by the output layer.

CNN models are generally applied for image processing and are widely known for extracting relevant features. However, one-dimensional convolutional filters (1D CNN) are used to analyze time series (Li et al., 2017). These filters slide over the input data to capture possible patterns in the time series. The main distinction of this technique over previous ANN models is that 1D CNN extracts features of a signal by considering local information rather than the entire signal in each network layer. The 1D CNN architecture used in this study consisted of the input layer, a hidden layer with 48 convolution filters (kernel size =3), a max-pooling layer (size = 2), a dense layer with 24 units and ReLU activation function, as shown in Fig. 4(b).

The input of the LSTM or CNN layer must be 3-dimensional following the format [samples, timesteps, features]. The timestep is equal to 30 days, the sample is equal to a row in a dataset (e.g., an input and output sequence for a time series), and the feature is input in the dataset. Therefore, the multivariate time series in this study were split into multiple samples where each sample has a specified number of time steps, and the output is ET_o at the last step. Thus, the input data dimension was [samples. 30, features]. The adam optimizer function (Kingma and Ba, 2015) was used to train the DL models and the best weights and biases were automatically loaded for testing. The Python library TensorFlow (TensorFlow Developers, 2021) was utilized to develop the ANN models. Two different combinations of input variables were used for each method, resulting in four DL models evaluated in this study. One model used inputs T_{min}, T_{max}, T_a, RH, U, and R_a, while the other model only had T_{min}, T_{max}, T_a, and R_a as input, as described in the previous section.

2.4. Performance assessment

The performance of the models was evaluated against CIMIS ET_o data, a modified version of the Penman equation (Pruitt and Doorenbos, 1977) that uses a wind function developed at the University of California, Davis, and unique cloud factor values for each station location. Five statistical indices, including the root mean squared error (RMSE), mean absolute error (MAE), mean bias error (MBE), Nash-Sutcliffe Efficiency (NSE), and coefficient of determination (R^2), were used to quantify and compare the performance of the temperature-based models.

$$RMSE = \sqrt{\frac{1}{n}\sum_{i=1}^{n}(E_i - M_i)^2} \tag{6}$$

$$MAE = \frac{1}{n}\sum_{i=1}^{n}|E_i - M_i| \tag{7}$$

$$MBE = \frac{1}{n}\sum_{i=1}^{n}(E_i - M_i) \tag{8}$$

$$NSE = 1 - \frac{\sum_{i=1}^{n}(M_i - E_i)^2}{\sum_{i=1}^{n}(E_i - \overline{E})^2} \tag{9}$$

$$R^2 = \left(\frac{\sum_{i=1}^{n}(E_i - \overline{E})(M_i - \overline{M})}{\sqrt{\sum_{i=1}^{n}(E_i - \overline{E})^2 \sum_{i=1}^{n}(M_i - \overline{M})^2}}\right)^2 \tag{10}$$

where E and M are the estimated and measured ET_o, respectively; $\overline{E}$ and $\overline{M}$ are the mean estimated and measured ET_o, respectively; and n is the total number of data points for each model. Monthly and annual error metrics were also computed to understand the performance of the models on a temporal scale. Linear regression calibration equations were also presented using long-term data from 101 CIMIS stations, as well as the stations from each climate division. Long-term ET_o data were interpolated using the inverse distance weighting approach in ArcGIS Pro 2.8.2 (ESRI Inc.) to assess the spatial distribution of the ET_o estimated by the models evaluated in this study.

Furthermore, the performance of these models was evaluated on 15 independent CIMIS stations during an independent period from 2020 to 2021 (Fig. 1) to validate the results.

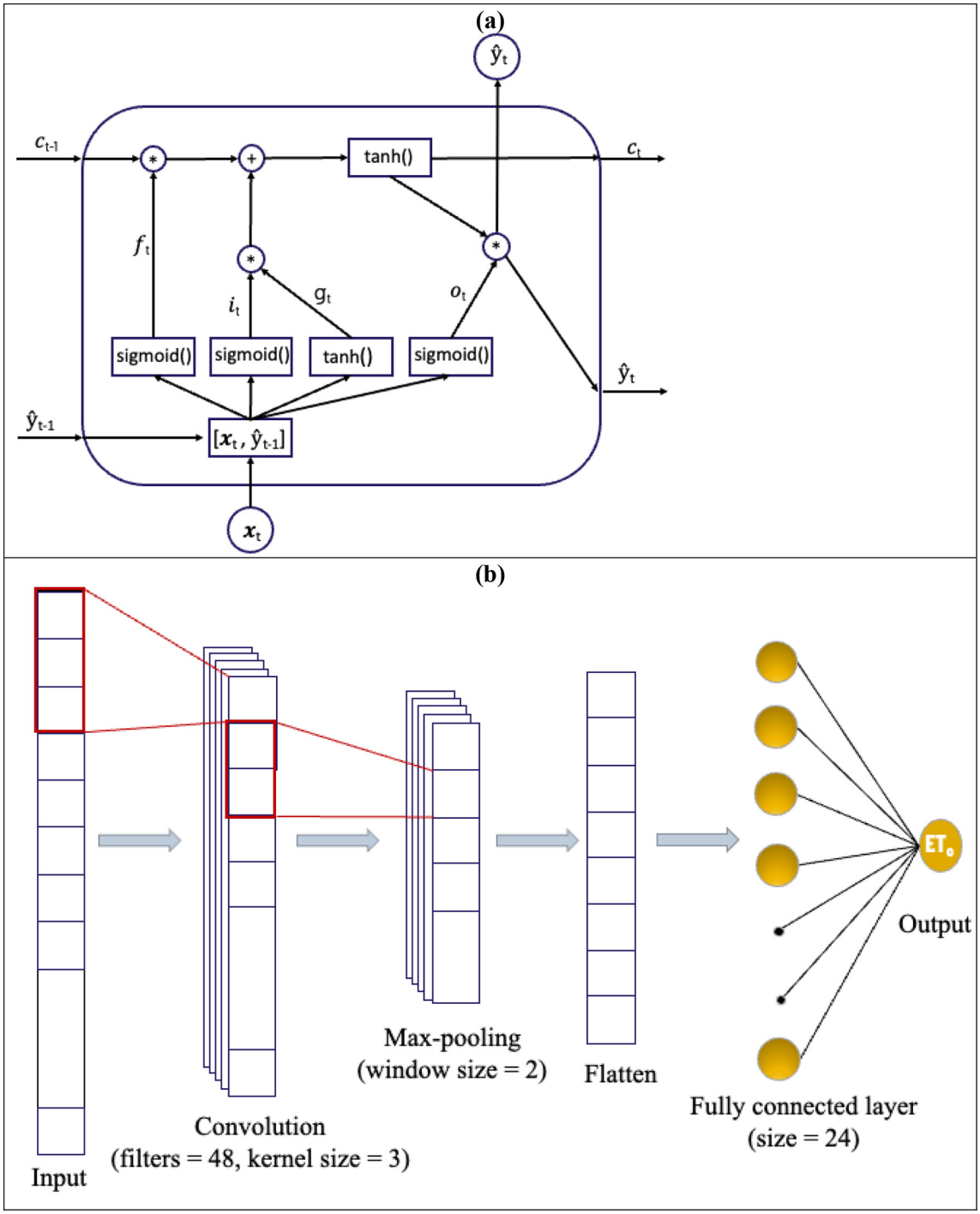

Fig. 4. A Long Short-Term Memory (LSTM) unit (a) and architecture of the 1D Convolutional Neural Network (CNN) used in this study (b).

3. Results & discussion

3.1. Overall performance of ET_o models

Table 1 summarizes the overall performance statistics of all the empirical regression and ANN-based ET_o models evaluated in this study. Fig. 5 shows the scatter plots of the ET_o estimated by the models against CIMIS ET_o. The HS model (RMSE = 0.78 mm d^{-1}; MAE = 0.56 mm d^{-1}) showed better performance among the empirical temperature-based models and resulted in a low magnitude of bias (MBE = −0.07 mm d^{-1}). Kukal et al. (2020) reported the underestimation of ET_o by the HS model in the arid, semi-arid, and dry subhumid sites of the US high plains region, while the overestimation of ET_o by the HS model was reported in the Sahelian climate by (Djaman et al., 2015). The BC model (RMSE = 0.91 mm d^{-1}; MAE = 0.67 mm d^{-1}), however resulted in overestimation of ET_o with MBE of 0.27 mm d-1. HS model has an NSE and R2 of 0.85 and 0.86, whereas it was 0.80 and 0.91, respectively for the BC model.

The ANN models can be ranked as ANN_all > ANN_T > WA-ANN_all > WA-ANN_T based on their performance. They showed high accuracy and reliability (generalizability), since data from the same CIMIS station was never present in the training and test set simultaneously. The ANN_all model (inputs: T_{min}, T_{max}, T_a, R_a, RH, U) showed the best performance (RMSE = 0.51 mm d^{-1}; MAE = 0.35 mm d^{-1}) followed

Table 1
Overall performance of the temperature-based ET_o models compared to CIMIS ET_o.

Models	Inputs	RMSE	MAE	MBE	NSE	R^2	Linear eq
BC	T_a, RH, Ud	0.91	0.67	0.27	0.80	0.91	y = 0.76× + 0.74
HS	T_{min}, $T_{max,}$ T_a, R_a	0.78	0.56	−0.07	0.85	0.86	y = 0.97× + 0.19
ANN_all	T_{min}, $T_{max,}$ T_a, R_a, RH, U	0.51	0.35	0.00	0.94	0.94	–
ANN_T	T_{min}, $T_{max,}$ T_a, R_a	0.69	0.49	0.00	0.88	0.88	–
WA-ANN_all	T_{min}, $T_{max,}$ T_a, R_a, RH, U	0.96	0.70	−0.01	0.78	0.78	–
WA-ANN_T	T_{min}, $T_{max,}$ T_a, R_a	0.99	0.73	0.00	0.77	0.77	–
LSTM_all	T_{min}, $T_{max,}$ T_a, R_a, RH, U	0.44	0.30	−0.01	0.95	0.95	–
LSTM_T	T_{min}, $T_{max,}$ T_a, R_a	0.67	0.47	0.02	0.89	0.89	–
CNN_all	T_{min}, $T_{max,}$ T_a, R_a, RH, U	0.46	0.32	0.00	0.95	0.95	–
CNN_T	T_{min}, $T_{max,}$ T_a, R_a	0.68	0.48	0.05	0.89	0.89	–

BC: Blaney & Criddle FAO, HS: Hargreaves & Samani, ANN_all: ANN model with T_{min}, T_{max}, T_a, R_a, RH, and U as inputs, WA-ANN_all: Wavelet transform ANN model with T_{min}, T_{max}, T_a, R_a, RH, and U as inputs, ANN_T: ANN model with T_{min}, T_{max}, T_a, and R_a as inputs, WA-ANN_T: wavelet transform ANN model with T_{min}, T_{max}, T_a, and R_a as inputs. LSTM_all: Long Short-Term Memory Recurrent Neural Network with 6 inputs, LSTM_T: 4 inputs, CNN_all: Convolutional neural network with 6 inputs, CNN_T: CNN model with 4 inputs, T_{min}, T_{max}, and T_a are in [°C], Relative Humidity, RH [%], daily average windspeed, U [m s^{-1}], Extraterrestrial solar radiation, R_a [mm d^{-1}].

by ANN-T (RMSE = 0.69 mm d^{-1}; MAE = 0.49 mm d^{-1}). WA-ANN models that used reconstructed signals obtained from the wavelet transform resulted in 69% higher error than ANN models that used raw data as input (Table 1). MBE values were negligible in all ANN models, indicating that there was no substantial over or underestimation of $ET_{o,}$ as shown in Fig. 5. The NSE and R^2 values ranged from 0.77 for the WA-ANN_T to 0.94 for the ANN_all models. Models using reconstructed signal obtained from the wavelet transform performed reasonably well with WA-ANN_all (RMSE = 0.96 mm d^{-1}; MAE = 0.70 mm d^{-1}) performing slightly better than WA-ANN_T (RMSE = 0.99 mm d^{-1}; MAE = 0.73 mm d^{-1}). Using the raw input data was a better approach than using the reconstructed signal in our study. This result agrees with the findings of (Falamarzi et al., 2014) but differs from the study by (Kisi and Alizamir, 2018), where ANN models with wavelet transform inputs did not have considerable differences from the models developed using raw inputs.

The DL models can be ranked as LSTM_all > CNN_all > LSTM_T > CNN_T based on their performance. They showed high reliability (generalization ability), since data from the same CIMIS station was never simultaneously present in the training and test set. The LSTM_all model (inputs: T_{min}, T_{max}, T_a, R_a, RH, U) showed the best performance (RMSE = 0.44 mm d^{-1}; MAE = 0.30 mm d^{-1}) followed by CNN-all (RMSE = 0.46 mm d^{-1}; MAE = 0.32 mm d^{-1}). Both the LSTM and CNN models had comparable performance. MBE values were negligible in all ANN models, indicating that there was no substantial over- or underestimation of $ET_{o,}$ as shown in Fig. 5. NSE and R^2 ranged from 0.89 for the models with four inputs to 0.95 for those using all six inputs.

Overall, the DL models with relative humidity, wind speed, air temperature, and extraterrestrial solar radiation as inputs surpassed other models in performance, such that LSTM_all >CNN_all >ANN_all. This was followed by models using air temperature and solar radiation as inputs such that LSTM_T > CNN_T > ANN_T > HS. All DL models outperformed the HS model with similar input variables. There was a 14%, 12%, and 11% decrease in RMSE for the LSTM_T, CNN_T, and ANN_T models, respectively, compared to HS. Better performance in estimating ET_o by ANN and WA-ANN models compared to HS was reported in the literature (Adamala, 2018; Traore et al., 2010). The superior performance of the LSTM and 1D CNN models agrees with the studies (Chen et al., 2020; Ferreira and da Cunha, 2020) where using a sequence of input variables (past information) to train the models resulted in an improved estimation of ET_o.

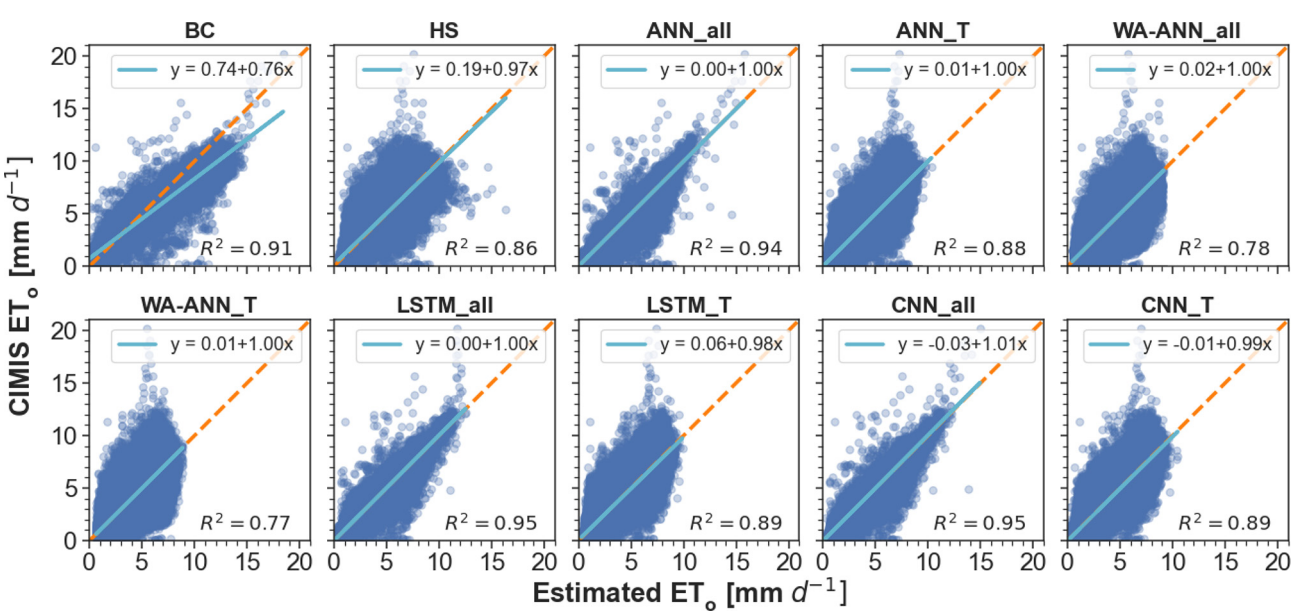

Fig. 5. Scatterplots of the CIMIS ET_o versus estimated daily ET_o by the 10 temperature-based empirical and DL models evaluated in this study. The dashed orange line is the 1:1 line. BC: Blaney & Criddle FAO, HS: Hargreaves & Samani, ANN_all: ANN model with T_{min}, T_{max}, T_a, R_a, RH, and U as inputs, WA-ANN_all: Wavelet transform ANN model with T_{min}, T_{max}, T_a, R_a, RH, and U as inputs, ANN_T: ANN model with T_{min}, T_{max}, T_a, and R_a as inputs, WA-ANN_T: wavelet transform ANN model with T_{min}, T_{max}, T_a, and R_a as inputs, LSTM_all: Long Short-Term Memory Recurrent Neural Network with 6 inputs, LSTM_T: 4 inputs, CNN_all: Convolutional neural network with 6 inputs, CNN_T: CNN with 4 inputs.

3.2. Importance of input parameters

HS model can be regarded as a truly temperature-based model since extraterrestrial solar radiation can be estimated based on the location and time of the year. Global solar radiation is known to be a more critical parameter than relative humidity and wind speed in estimating daily ET_o, based on a machine learning study conducted in China (Fan et al., 2018). However, daily ET_o anomalies strongly correlate with net radiation anomalies, relative humidity (RH), and cloud cover, and less with average daily air temperature (Hidalgo et al., 2005). The temperature difference used in the HS model is an indirect measure of cloud cover and RH at a location (Hargreaves and Samani, 1985). Clear sky conditions result in high maximum day temperatures and low minimum night temperatures, whereas cloudy days result in relatively lower maximum day temperatures and higher minimum night temperatures.

In our study, the ANN_all model using relative humidity, wind speed, air temperature, and extraterrestrial solar radiation resulted in better performance (27% reduction in MAE) than ANN_T, based on temperature and extraterrestrial solar radiation. However, ANN_all requires more data, typically unavailable for ET_o estimation by smart controllers in residential areas. Many studies, with few exceptions, use R_s as an input to temperature-based models instead of R_a. Since we used R_a as an additional input for the temperature-based models, which can be calculated following the equations given by Allen et al. (1998), the temperature is the only measured input required for temperature-based models developed in this study. Partal (2009) reported no improvement in performance by the ANN and WA-ANN models over the HS model. On the contrary, the ANN_T model in our study resulted in a 14% reduction in MAE compared to the empirical HS model derived from the same inputs.

Studies using DL models have reported great performance for ET_o estimation using solar radiation and temperature as inputs (Elbeltagi et al., 2020; Sowmya et al., 2020). Sowmya et al. (2020) used deep feedforward ANN models for ET_o estimation at two CIMIS stations and found that global solar radiation and air temperature can provide comparable accuracy to the models using a complete set of weather variables as inputs. In our study however, DL models trained with a complete set of variables resulted in better performance (~35% reduction in MAE) than models using four inputs, although the performance of DL models trained with four inputs was not substantially lower. Therefore, temperature-based DL can be adopted to obtain accurate ET_o estimations for landscape irrigation management by smart weather-based irrigation controllers in data-scarce conditions in urban settings.

3.3. Temporal analysis of the ET_o models

Fig. 6 shows the daily mean and standard deviation of the estimated ET_o values throughout the year by the models evaluated in this study versus the CIMIS ET_o. The monthly performance statistics for each model to estimate the monthly average ET_o are shown in Tables 2 to 4. The HS (MAE: 0.10 to 0.31 mm d^{-1}) model consistently performed better throughout the year; however, had a high error in the spring months relative to other months. The BC model (MAE: 0.08 to 0.76 mm d^{-1}) model had a performance comparable to that of the HS model in the winter and spring months but performed poorly in the summer months, also evident in Fig. 6.

The ANN-based models can be ranked as ANN_all > ANN_T > WA-ANN_all >WA-ANN_T. The ANN models showed negligible bias throughout the year, with MBE ranging from −0.23 to 0.13 mm d^{-1}, whereas MBE ranged from −0.3 to 0.05 mm d^{-1} for the HS empirical model (Tables 2 to 4). MAE values ranged from 0.05 to 0.14 mm d^{-1} for the ANN models and from 0.13 to 0.29 mm d^{-1} for the WA-ANN models. The better performance of the ANN models is also apparent in Fig. 6, where the mean and standard deviation of the estimated ET_o very closely to that of the CIMIS ET_o throughout the year.

The DL models can be ranked as LSTM_all > CNN_all > LSTM_T > CNN_T. All models showed negligible bias throughout the year, with MBE ranging from −0.06 to 0.08 mm d^{-1}, better than the empirical and other ML models evaluated in this study (Tables 2 to 4). MAE values ranged from 0.04 to 0.11 mm d^{-1} for the LSTM models and from 0.05 to 0.13 mm d^{-1} for the CNN models. The better performance of the DL models is also apparent in Fig. 6, where the mean and standard deviation of the estimated ET_o match very closely with that of the CIMIS ET_o throughout the year.

The relationship of MAE and MBE with the annual average of the meteorological parameters, including wind speed, was different. The

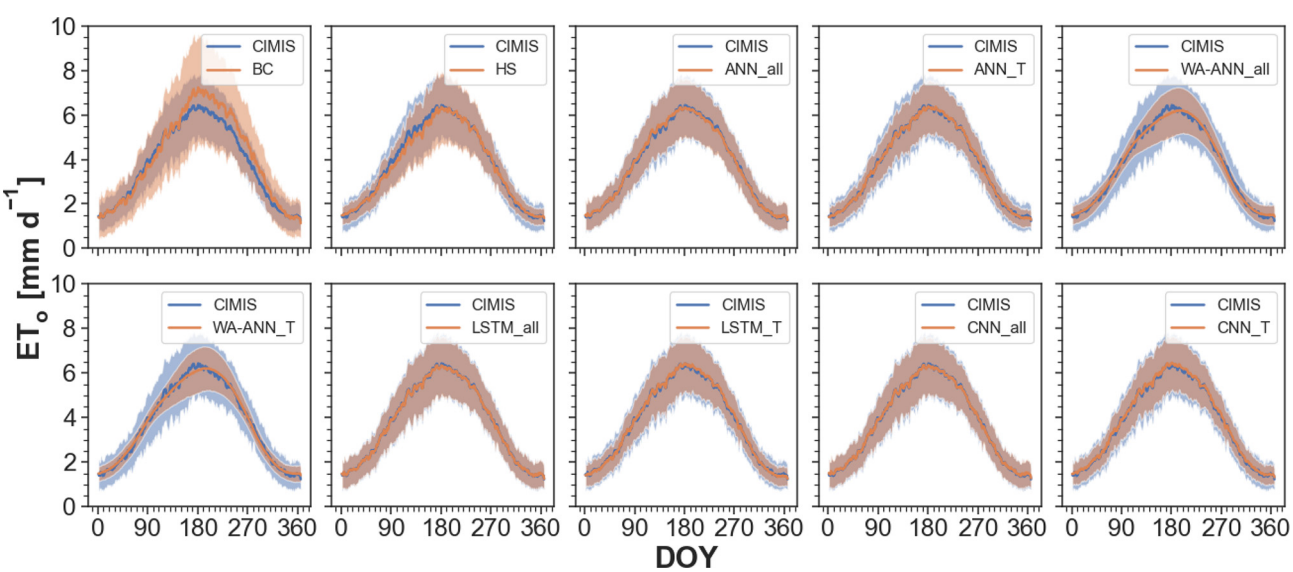

Fig. 6. Comparison between long-term year-round ET_o obtained from CIMIS against the 10 temperature-based empirical and DL ET_o models evaluated in this study. The solid lines show mean ET_o and the shaded bands depict the standard deviation of ET_o across all CIMIS stations. DOY: day of the year. BC: Blaney & Criddle FAO, HS: Hargreaves & Samani, ANN_all: ANN model with T_{min}, T_{max}, T_a, R_a, RH, and U as inputs, WA-ANN_all: Wavelet transform ANN model with T_{min}, T_{max}, T_a, R_a, RH, and U as inputs, ANN_T: ANN model with T_{min}, T_{max}, T_a, and R_a as inputs, WA-ANN_T: wavelet transform ANN model with T_{min}, T_{max}, T_a, and R_a as inputs, LSTM_all: Long Short-Term Memory Recurrent Neural Network with 6 inputs, LSTM_T: 4 inputs, CNN_all: Convolutional neural network with 6 inputs, CNN_T: CNN with 4 inputs.

Table 2
Monthly root mean square error, RMSE (mm d^{-1}) values for the temperature-based ET_o equations evaluated in this study against CIMIS ET_o.

Model	Jan	Feb	Mar	Apr	May	Jun	Jul	Aug	Sep	Oct	Nov	Dec
BC	0.15	0.15	0.24	0.23	0.22	0.61	0.79	0.70	0.69	0.53	0.25	0.11
HS	0.13	0.13	0.20	0.34	0.33	0.24	0.16	0.12	0.13	0.13	0.15	0.12
ANN_all	0.08	0.08	0.09	0.14	0.16	0.13	0.13	0.16	0.09	0.10	0.07	0.08
ANN_T	0.11	0.11	0.15	0.16	0.16	0.16	0.13	0.13	0.12	0.15	0.14	0.14
WA-ANN_all	0.16	0.21	0.21	0.26	0.20	0.34	0.23	0.24	0.20	0.31	0.20	0.21
WA-ANN_T	0.16	0.22	0.22	0.26	0.23	0.33	0.21	0.25	0.23	0.31	0.21	0.21
LSTM_all	0.06	0.08	0.08	0.10	0.10	0.13	0.12	0.14	0.09	0.09	0.07	0.06
LSTM_T	0.21	0.15	0.15	0.14	0.14	0.13	0.13	0.13	0.13	0.12	0.14	0.14
CNN_all	0.08	0.08	0.08	0.10	0.11	0.14	0.11	0.14	0.09	0.09	0.07	0.07
CNN_T	0.19	0.13	0.16	0.15	0.16	0.15	0.14	0.12	0.13	0.12	0.14	0.13

BC: Blaney & Criddle FAO, HS: Hargreaves & Samani, ANN_all: ANN model with T_{min}, T_{max}, T_a, R_a, RH, and U as inputs, WA-ANN_all: Wavelet transform ANN model with T_{min}, T_{max}, T_a, R_a, RH, and U as inputs, ANN_T: ANN model with T_{min}, T_{max}, T_a, and R_a as inputs, WA-ANN_T: wavelet transform ANN model with T_{min}, T_{max}, T_a, and R_a as inputs, LSTM_all: Long Short-Term Memory Recurrent Neural Network with 6 inputs, LSTM_T: 4 inputs, CNN_all: Convolutional neural network with 6 inputs, CNN_T: CNN model with 4 inputs.

Table 3
Monthly mean absolute error, MAE (mm d^{-1}) values for the temperature-based ET_o equations evaluated in this study against CIMIS ET_o.

Model	Jan	Feb	Mar	Apr	May	Jun	Jul	Aug	Sep	Oct	Nov	Dec
BC	0.11	0.14	0.20	0.20	0.17	0.57	0.76	0.69	0.67	0.51	0.22	0.08
HS	0.11	0.10	0.16	0.31	0.28	0.21	0.13	0.10	0.11	0.11	0.11	0.10
ANN_all	0.06	0.06	0.07	0.10	0.14	0.10	0.10	0.12	0.08	0.08	0.06	0.05
ANN_T	0.08	0.09	0.11	0.12	0.12	0.13	0.10	0.09	0.09	0.11	0.10	0.10
WA-ANN_all	0.13	0.17	0.16	0.19	0.16	0.29	0.18	0.19	0.16	0.24	0.15	0.15
WA-ANN_T	0.14	0.18	0.16	0.20	0.18	0.27	0.17	0.20	0.18	0.23	0.15	0.15
LSTM_all	0.05	0.06	0.06	0.07	0.08	0.10	0.09	0.09	0.07	0.06	0.05	0.04
LSTM_T	0.11	0.10	0.11	0.11	0.11	0.09	0.10	0.09	0.11	0.10	0.09	0.10
CNN_all	0.06	0.06	0.06	0.08	0.09	0.10	0.09	0.09	0.07	0.06	0.05	0.05
CNN_T	0.11	0.10	0.11	0.11	0.13	0.11	0.11	0.09	0.11	0.09	0.10	0.09

BC: Blaney & Criddle FAO, HS: Hargreaves & Samani, ANN_all: ANN model with T_{min}, T_{max}, T_a, R_a, RH, and U as inputs, WA-ANN_all: Wavelet transform ANN model with T_{min}, T_{max}, T_a, R_a, RH, and U as inputs, ANN_T: ANN model with T_{min}, T_{max}, T_a, and R_a as inputs, WA-ANN_T: wavelet transform ANN model with T_{min}, T_{max}, T_a, and R_a as inputs, LSTM_all: Long Short-Term Memory Recurrent Neural Network with 6 inputs, LSTM_T: 4 inputs, CNN_all: Convolutional neural network with 6 inputs, CNN_T: CNN model with 4 inputs.

HS model tended to have higher MAE with increasing wind speed, vapor pressure deficit, and global solar radiation. Similarly, HS tends to have a lower MAE with increasing relative humidity, whereas these trends were not clear for the BC model. In the same way, HS tend to underestimate ET_o with increasing wind speed, vapor pressure deficit, and global solar radiation, as indicated by the decreasing MBE. Furthermore, with increasing relative humidity, HS overestimates ET_o, whereas MBE changed negligibly for the BC model. The HS model tended to underestimate ET_o under high wind conditions (> 3 m s^{-1}) and overestimate ET_o under conditions of high relative humidity (Allen et al., 1998), which is also supported by our results. Reasons may include the continual mixing of warm, dry air from overhead into the equilibrium boundary layer at night, reducing the difference between the maximum and minimum air temperature values (Temesgen et al., 1999).

3.4. Spatial analysis of ET_o models

Table 5 summarizes the performance of the models evaluated in this study for each climate division. Also shown in Table 5 are the coefficients (i.e., A and B) of BC_{fao} averaged for each climate division. The average values of these coefficients across all CIMIS stations were $A = -1.96$ and $B = 1.37$. Based on the effects of weather variables on annual ET_o (Figs. 7 and 8), it can be expected that the performance of temperature-based ET_o equations will vary based on climate, i.e., more arid regions will tend to have higher error. The southeast desert basin had the highest error among all climate divisions as it is the aridest region of the state (Table 5).

The HS model was the best performing empirical model in all climate divisions with the MAE ranging from 0.47 to 0.73 mm d^{-1}. Gabriela Arellano and Irmak (2016) reported an underestimation of

Table 4
Monthly mean bias error, MBE (mm d^{-1}) values for the temperature-based ET_o equations evaluated in this study against CIMIS ET_o.

Model	Jan	Feb	Mar	Apr	May	Jun	Jul	Aug	Sep	Oct	Nov	Dec
BC	−0.06	−0.10	−0.19	−0.17	0.11	0.57	0.76	0.69	0.67	0.51	0.20	−0.04
HS	0.05	−0.02	−0.14	−0.30	−0.28	−0.18	−0.01	−0.02	0.04	−0.02	0.03	0.02
ANN_all	0.03	0.01	0.02	0.08	0.12	0.00	−0.05	−0.11	−0.03	−0.06	−0.02	0.02
ANN_T	−0.01	−0.02	0.01	−0.02	0.00	−0.05	0.02	−0.01	0.04	−0.05	−0.02	−0.05
WA-ANN_all	0.06	0.02	0.01	0.01	−0.04	−0.23	−0.06	0.04	0.03	−0.20	−0.04	0.06
WA-ANN_T	0.05	0.03	0.02	−0.04	−0.08	−0.19	−0.01	0.07	0.06	−0.16	−0.03	0.04
LSTM_all	0.01	−0.01	−0.01	0.00	−0.01	−0.04	−0.05	−0.05	−0.01	−0.03	−0.01	0.01
LSTM_T	−0.06	−0.06	0.01	0.02	0.04	0.03	0.06	0.03	0.07	−0.02	−0.04	−0.06
CNN_all	0.04	0.01	0.01	0.02	0.02	−0.02	−0.04	−0.06	−0.01	−0.03	−0.01	0.03
CNN_T	0.01	0.01	0.04	0.03	0.07	0.06	0.08	0.01	0.07	0.01	0.02	0.01

BC: Blaney & Criddle FAO, HS: Hargreaves & Samani, ANN_all: ANN model with T_{min}, T_{max}, T_a, R_a, RH, and U as inputs, WA-ANN_all: Wavelet transform ANN model with T_{min}, T_{max}, T_a, R_a, RH, and U as inputs, ANN_T: ANN model with T_{min}, T_{max}, T_a, and R_a as inputs, WA-ANN_T: wavelet transform ANN model with T_{min}, T_{max}, T_a, and R_a as inputs, LSTM_all: Long Short-Term Memory Recurrent Neural Network with 6 inputs, LSTM_T: 4 inputs, CNN_all: Convolutional neural network with 6 inputs, CNN_T: CNN model with 4 inputs.

Table 5
Climate-division-specific calibration equations and performance statistics for the temperature-based ET_o equations and deep learning models evaluated in this study against CIMIS ET_o.

Climate Division	ET Model	linear fit	R^2	NSE	RMSE	MAE	MBE
401	BC	y = 0.86× + 0.60	0.92	0.89	0.61	0.47	−0.13
(North Coast Drainage)	HS	y = 0.95× + 0.05	0.88	0.88	0.64	0.47	0.11
$n = 10$	ANN_all		0.94	0.94	0.45	0.31	0
A = −1.91	ANN_T		0.9	0.9	0.58	0.4	0.15
B = 1.29	WA-ANN_all		0.77	0.75	0.91	0.67	0.22
	WA-ANN_T		0.77	0.73	0.94	0.68	0.3
	LSTM_all		0.95	0.95	0.39	0.28	−0.03
	LSTM_T		0.91	0.9	0.56	0.39	0.12
	CNN_all		0.95	0.95	0.42	0.3	0
	CNN_T		0.91	0.9	0.58	0.41	0.16
402	BC	y = 0.77× + 0.59	0.94	0.83	0.9	0.67	0.38
(Sacramento Drainage)	HS	y = 0.99× + 0.22	0.85	0.84	0.87	0.62	−0.19
$n = 11$	ANN_all		0.95	0.95	0.47	0.32	0.03
A = −1.97	ANN_T		0.88	0.88	0.75	0.53	−0.11
B = 1.42	WA-ANN_all		0.8	0.8	0.98	0.71	−0.01
	WA-ANN_T		0.78	0.78	1.02	0.73	0.02
	LSTM_all		0.97	0.96	0.41	0.28	−0.01
	LSTM_T		0.88	0.88	0.75	0.53	−0.08
	CNN_all		0.96	0.96	0.44	0.31	0.01
	CNN_T		0.88	0.88	0.75	0.54	−0.03
403	BC	y = 0.76× + 0.97	0.94	0.85	0.83	0.67	0.01
(Northeast Interior Basis)	HS	y = 0.94× + 0.49	0.88	0.86	0.78	0.58	−0.28
n = 1	ANN_all		0.93	0.93	0.57	0.39	0.15
A = −1.99	ANN_T		0.9	0.89	0.7	0.51	−0.19
B = 1.49	WA-ANN_all		0.77	0.77	1.01	0.75	−0.08
	WA-ANN_T		0.75	0.74	1.09	0.78	0.02
	LSTM_all		0.95	0.95	0.46	0.32	0.08
	LSTM_T		0.9	0.89	0.69	0.51	−0.19
	CNN_all		0.95	0.95	0.49	0.34	0.04
	CNN_T		0.89	0.89	0.71	0.52	−0.12
404	BC	y = 0.88× + 0.62	0.87	0.84	0.66	0.51	−0.24
(Central Coast Drainage)	HS	y = 1.01× + 0.16	0.84	0.83	0.68	0.52	−0.18
$n = 20$	ANN_all		0.9	0.89	0.53	0.4	−0.13
A = −1.86	ANN_T		0.87	0.87	0.59	0.45	−0.1
B = 1.23	WA-ANN_all		0.7	0.68	0.92	0.69	0.22
	WA-ANN_T		0.69	0.67	0.94	0.7	0.23
	LSTM_all		0.92	0.92	0.46	0.33	−0.07
	LSTM_T		0.88	0.88	0.58	0.42	−0.06
	CNN_all		0.92	0.92	0.48	0.35	−0.04
	CNN_T		0.87	0.87	0.59	0.44	−0.03
405	BC	y = 0.77× + 0.54	0.96	0.83	0.95	0.7	0.5
(San Joaquin Drainage)	HS	y = 1.01× - 0.05	0.9	0.9	0.73	0.52	0.02
$n = 23$	ANN_all		0.96	0.96	0.45	0.31	0.02
A = −1.98	ANN_T		0.92	0.92	0.65	0.46	0.05
B = 1.42	WA-ANN_all		0.86	0.86	0.85	0.61	−0.01
	WA-ANN_T		0.85	0.85	0.88	0.64	−0.06
	LSTM_all		0.97	0.97	0.38	0.26	0
	LSTM_T		0.92	0.92	0.64	0.45	0.08
	CNN_all		0.97	0.97	0.4	0.28	0
	CNN_T		0.92	0.92	0.65	0.46	0.1
406	BC	y = 0.82× + 0.57	0.85	0.81	0.72	0.55	0.09
(South Coast Drainage)	HS	y = 0.94× + 0.31	0.8	0.79	0.76	0.56	−0.08
$n = 21$	ANN_all		0.88	0.88	0.56	0.4	−0.01
A = −1.93	ANN_T		0.83	0.82	0.7	0.5	0.05
B = 1.32	WA-ANN_all		0.64	0.64	1	0.76	−0.04
	WA-ANN_T		0.63	0.62	1.01	0.76	0.01
	LSTM_all		0.91	0.91	0.49	0.34	0.02
	CNN_all		0.91	0.9	0.51	0.36	0.04
	CNN_T		0.83	0.83	0.69	0.49	0.08
407	BC	y = 0.72× + 0.64	0.92	0.58	1.47	1.15	0.99
(Southeast Desert Basin)	HS	y = 0.90× + 0.55	0.81	0.8	1.03	0.73	−0.06
$n = 15$	ANN_all		0.95	0.94	0.54	0.33	0.13
A = −2.10	WA-ANN_all		0.77	0.74	1.17	0.86	−0.44
B = 1.60	WA-ANN_T		0.75	0.71	1.22	0.91	−0.46
	LSTM_all		0.96	0.96	0.48	0.31	0.01
	LSTM_T		0.86	0.86	0.86	0.6	−0.01
	CNN_all		0.95	0.95	0.51	0.34	0.02
	CNN_T		0.86	0.86	0.87	0.6	0

BC: Blaney & Criddle FAO, HS: Hargreaves & Samani, ANN_all: ANN model with T_{min}, T_{max}, T_a, R_a, RH, and U as inputs, WA-ANN_all: Wavelet transform ANN model with T_{min}, T_{max}, T_a, R_a, RH, and U as inputs, ANN_T: ANN model with T_{min}, T_{max}, T_a, and R_a as inputs, WA-ANN_T: wavelet transform ANN model with T_{min}, T_{max}, T_a, and R_a as inputs, LSTM_all: Long Short-Term Memory Recurrent Neural Network with 6 inputs, LSTM_T: 4 inputs, CNN_all: Convolutional neural network with 6 inputs, CNN_T: CNN with 4 inputs, n: the number of CIMIS stations in each climate division. A and B: coefficients of the BC model.

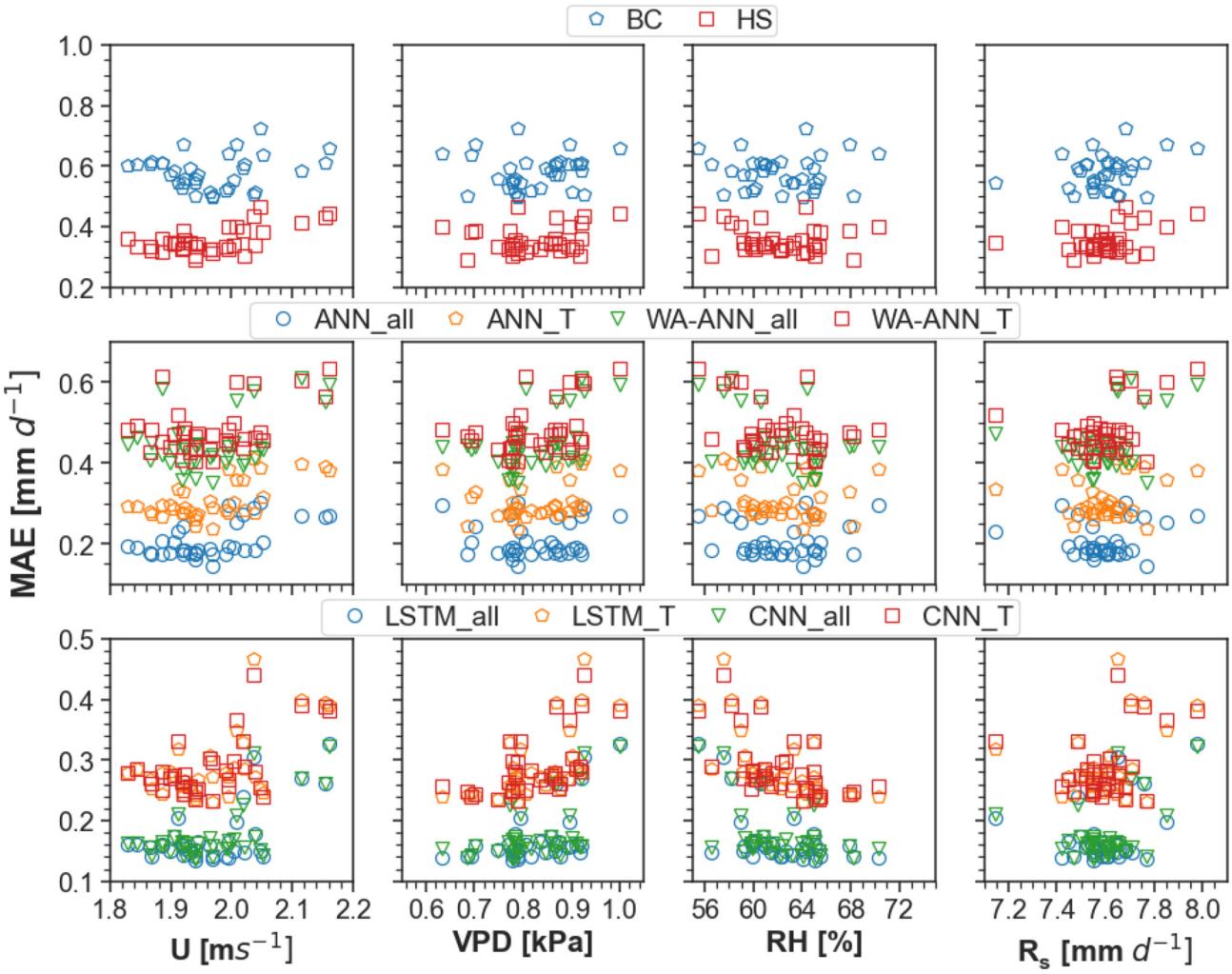

Fig. 7. Variation in annual mean absolute error, MAE [mm d^{-1}] values against meteorological variables - wind speed (U), relative humidity (RH), vapor pressure deficit (VPD), and global solar radiation (R_s).

ET_o and RMSE of 1.0 mm d^{-1} for the HS model at CIMIS Station 6 in the Sacramento drainage region. This is in close agreement with the results of our study with RMSE of 0.87 mm d^{-1} and the underestimation (MBE = −20 mm d^{-1}) of ET_o, as is also evident in Fig. 9. The BC model (MAE: 0.47 to 1.15 mm d^{-1}) performed relatively better in the coastal regions, i.e., north coast drainage, central coast drainage, and south coast drainage, where its performance was similar to the HS model. This can also be observed in Fig. 9, where the mean ET_o estimated by the BC model is similar to the CIMIS ET_o in the coastal regions. NSE ranged from 0.58 (in the southeast desert basin) to 0.89 (in north coast drainage) for the BC model, and from 0.79 (in south coast drainage) to 0.90 (in san joaquin drainage) for the HS model. R^2 varied from 0.85 (in south coast drainage) to 0.96 (in San Joaquin drainage) for the BC model, and from 0.80 (in south coast drainage) to 0.90 (in san joaquin drainage).

The mean long-term CIMIS ET_o ranged from 2.58 mm d^{-1} (at CIMIS #193 in the central coast drainage) to 5.29 mm d^{-1} (CIMIS # 200 in the southeast desert basin) (Fig. 9). The mean ET_o ranged from 2.05 to 6.91 mm d^{-1} for the temperature-based empirical models, with the lowest (at CIMIS # 193 in central coast drainage) and highest (at CIMIS # 200 in the southeast desert basin) observed for the BC model (Fig. 9).

The ANN models can be ranked as ANN_all >ANN_T > WA-ANN_all > WA-ANN_T, based on their performance in the climate divisions. MAE ranged from 0.31 mm d-1 (ANN_all in the north-coast drainage) to 0.91 mm d^{-1} (WA-ANN_T in the southeast desert basin) for the ANN models. The MBE values ranged from −0.46 mm d^{-1} (WA-ANN_T in the southeast desert basin) to 0.30 mm d^{-1} (WA-ANN_T in the north coast drainage). NSE ranged from 0.62 (WA-ANN_T in the south coast drainage) to 0.96 (ANN_all in the San Joaquin drainage), and R^2 values varied from 0.63 (WA-ANN_T in the south coast drainage) to 0.96 (ANN_all in the San Joaquin drainage). The mean ET_o values ranged from 2.24 mm d^{-1} (at CIMIS #193 in the central coast drainage) to 5.42 mm d^{-1} (CIMIS # 200 in the southeast desert basin) for the models ANN_T and ANN_all, respectively (Fig. 9). ANN_T model, which used the same inputs as the HS model, resulted in a reduction of MAE ranging from 11% to 17% in all climate divisions, thus offering a promising alternative for accurate estimations of ET_o.

Similarly, DL models can be ranked as LSTM_all > CNN_all > LSTM_T > CNN_T, based on their performance in the climate divisions. MAE ranged from 0.26 mm d^{-1} (LSTM_all in San Joaquin drainage) to 0.60 mm d^{-1} (CNN_T in the southeast desert basin). The MBE values ranged from −0.19 mm d^{-1} (LSTM_T in the northeast interior basin) to 0.16 mm d^{-1} (CNN_T in north coast drainage). The NSE and R^2 values varied from 0.83 (CNN_T in the South Coast drainage) to 0.97 (LSTM_all in the San Joaquin drainage). Long-term mean ET_o values ranged from 2.43 mm d^{-1} (at CIMIS #193 in central coast drainage) to 5.26 mm d^{-1} (CIMIS # 200 in the southeast desert basin) observed for the LSTM_all model (Fig. 9). The LSTM_T and CNN_T models, which used the same inputs as the HS model, resulted in a reduction of MAE ranging

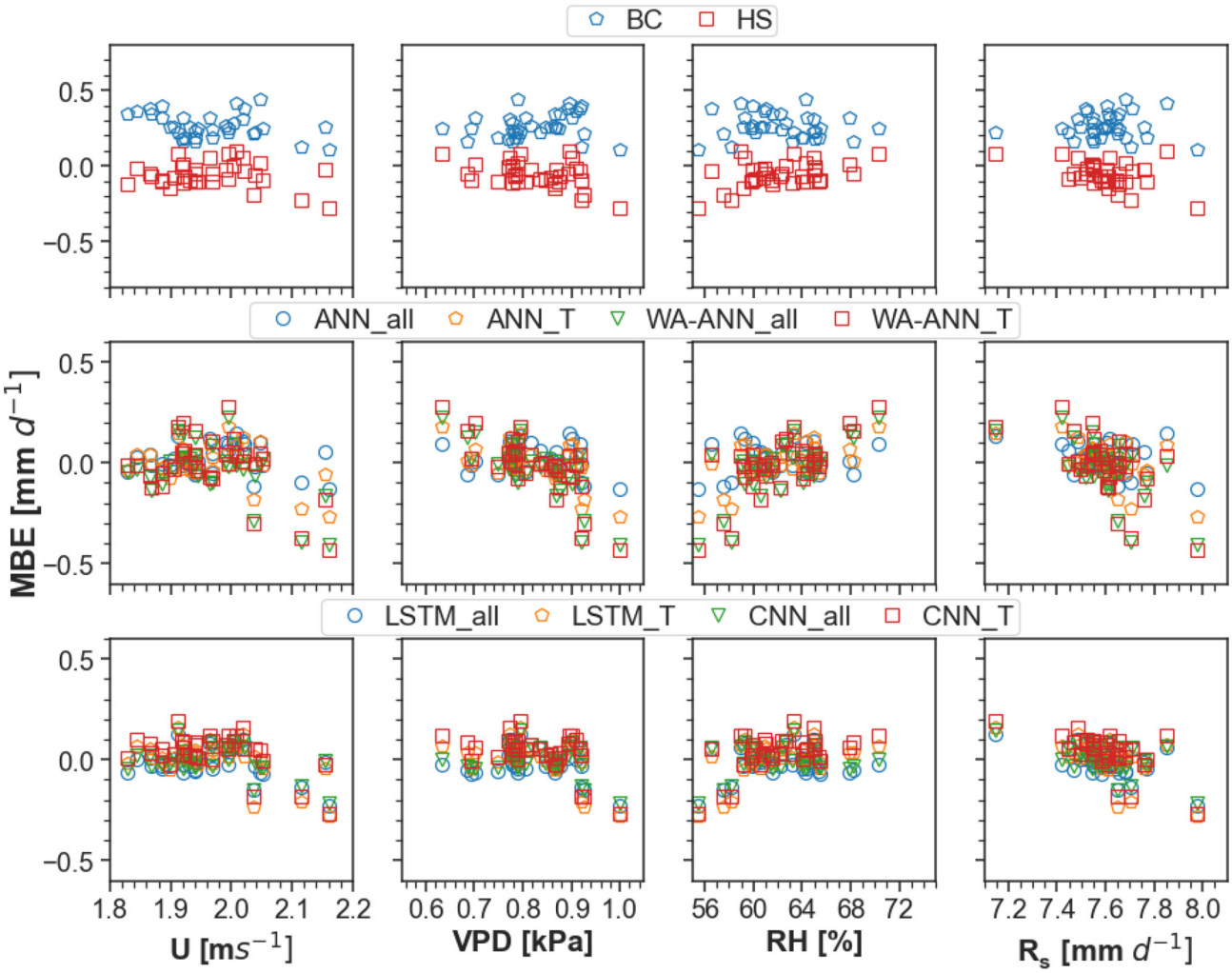

Fig. 8. Variation in annual mean bias error, MBE [mm d^{-1}] values against meteorological variables - wind speed (U), relative humidity (RH), vapor pressure deficit (VPD), and global solar radiation (R_s). BC: Blaney & Criddle FAO, HS: Hargreaves & Samani, ANN_all: ANN model with T_{min}, T_{max}, T_a, R_a, RH, and U as inputs, WA-ANN_all: Wavelet transform ANN model with T_{min}, T_{max}, T_a, R_a, RH, and U as inputs, ANN_T: ANN model with T_{min}, T_{max}, T_a, and R_a as inputs, WA-ANN_T: wavelet transform ANN model with T_{min}, T_{max}, T_a, and R_a as inputs, LSTM_all: Long Short-Term Memory Recurrent Neural Network with 6 inputs, LSTM_T: 4 inputs, CNN_all: Convolutional neural network with 6 inputs, CNN_T: CNN with 4 inputs.

from 10% to 18% in all climate divisions, thus offering a promising alternative for accurate estimations of ET_o using only temperature as input.

3.5. Validation

Table 6 shows the performance indices of the original/calibrated empirical models and the DL models developed in this study. Since wavelet analysis ANN models resulted in the worst performance compared to other DL models, these models are excluded from the validation. Empirical models calibrated using the coefficients presented in Tables 1 and 5 were evaluated at the validation sites. This analysis was performed to indirectly account for the meteorological variables not used in the Hargreaves equations, such as RH and U. Fig. 10 shows the box plots for the models evaluated at the validation sites. We observed that the climate division-specific calibration, HS(cal_{cd}) with MAE = 0.66 mm d^{-1}, performed slightly better than the original HS model (MAE = 0.68 mm d^{-1}) which also concurs with the results from other studies (Kukal et al., 2020; Senatore et al., 2020); however, the performance improvement was not substantial in our study. The original BC model requires information about relative humidity and wind speed as shown in Eqs. 2 and 3. We obtained the average value of BC coefficients *A* and *B* from 101 CIMIS stations and used these values to calculate BC(cal), while the climate division-specific average was used to calculate BC (cal_{cd}). BC(cal_{cd}) with MAE = 0.86 mm d^{-1} resulted in comparable performance to the original BC model (MAE = 0.81 mm d^{-1}) for the validation sites.

On the other hand, temperature-based DL models showed improved performance with ANN_T (MAE = 0.57 mm d^{-1}), LSTM_T (MAE = 0.54 mm d^{-1}), and CNN_T (MAE = 0.56 mm d^{-1}), resulting in a 15%, 20%, and 17% reduction in the MAE, respectively, compared to the HS (cal_{cd}) model. The performance indices for the other DL models using all weather inputs are also shown in Table 6. It is deduced that deep learning models can help estimate ET_o at a new location accurately. Furthermore, including the temporal information as inputs, for example, in LSTM and CNN-1D models, does not result in a substantial improvement in performance compared to ANN models.

Readers should note that this paper only focused on ET_o derived from CIMIS stations because of its widespread use in irrigation scheduling and availability in various climate conditions (Fig. 1). Meteorological data, specifically temperature data, are available from the highly dense network of stations from National Centers for Environmental Information (NCEI) by the National Oceanic and Atmospheric Administration (NOAA). However, most ET_o equations are developed using data from irrigated agriculture crops, and CIMIS measures meteorological variables in a "standardized condition" on a well-watered extended surface of green grass. In contrast, public weather sites often lie adjacent to

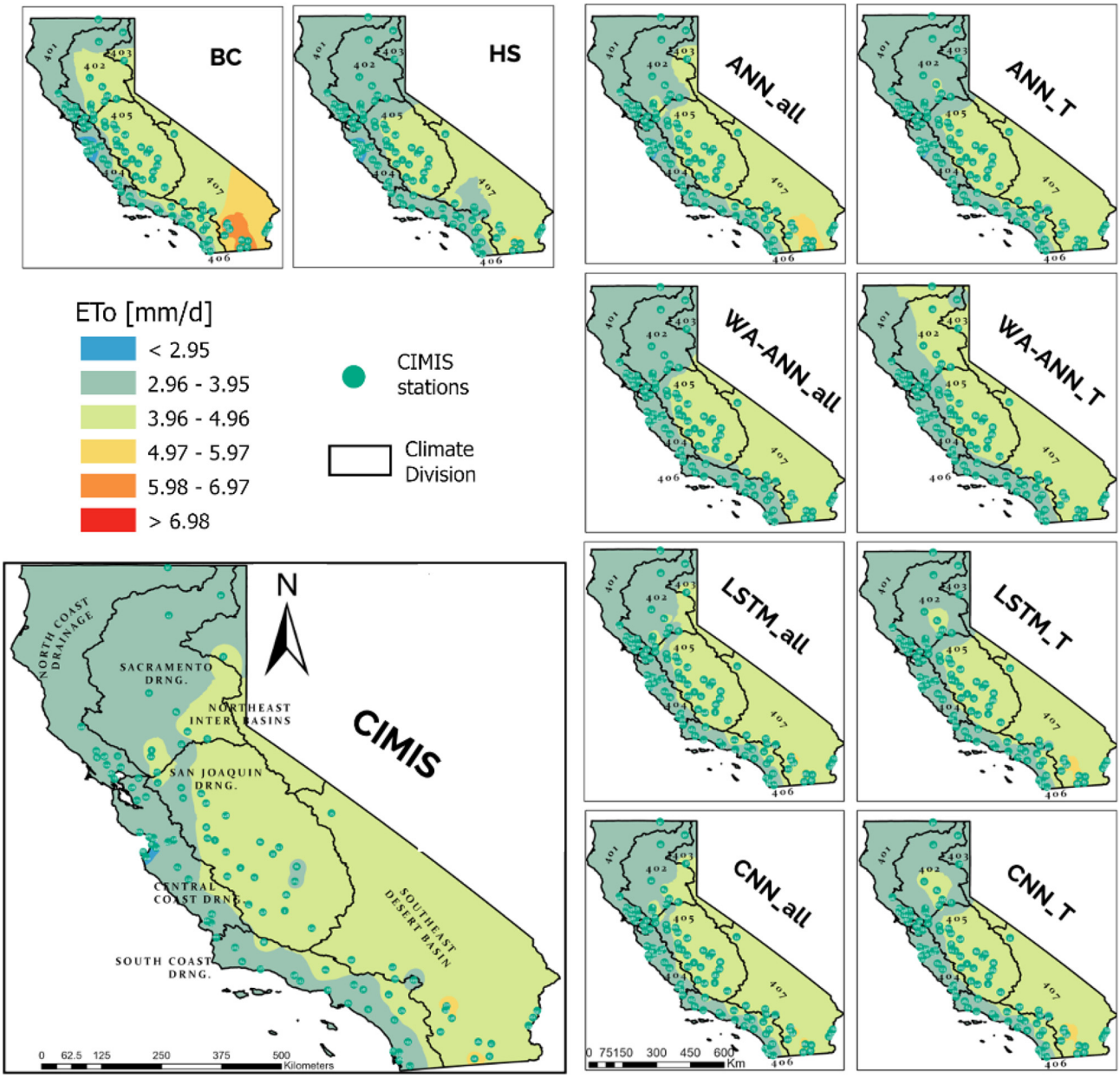

Fig. 9. Comparison between the long-term ET_o maps obtained from CIMIS against the estimated maps by the temperature-based empirical and DL models evaluated in this study. BC: Blaney & Criddle FAO, HS: Hargreaves & Samani, ANN_all: ANN model with T_{min}, T_{max}, T_a, R_a, RH, and U as inputs, WA-ANN_all: Wavelet transform ANN model with T_{min}, T_{max}, T_a, R_a, RH, and U as inputs, ANN_T: ANN model with T_{min}, T_{max}, T_a, and R_a as inputs, WA-ANN_T: wavelet transform ANN model with T_{min}, T_{max}, T_a, and R_a as inputs, LSTM_all: Long hort-Term Memory Recurrent Neural Network with 6 inputs, LSTM_T: 4 inputs, CNN_all: Convolutional neural network with 6 inputs, CNN_T: CNN model with 4 inputs.

asphalt, oiled or graveled lots, streets, roads, roofed structures, or within non-irrigated, non-cultivated lands (Allen and Pruitt, 1986). This must be considered since the choice of the ET_o equation depends significantly on the origin and the environmental conditions of its development. Therefore, future work in regional/site-specific calibration of temperature-based empirical models using data from these stations might be helpful (Kukal et al., 2020; Long et al., 2013; Senatore et al., 2020).

4. Conclusion

This study evaluated the performance of deep learning (DL) and two empirical temperature-based ET_o models at 101 active California Irrigation Management Information System (CIMIS) weather stations in California, using >725,000 observations from 1985 to 2019. The DL models outperformed the empirical equations and showed high generalizability when evaluated on the independent sites. Our results suggest that using raw input data for ANN models is better than using the reconstructed signal obtained from the wavelet transform. Furthermore, using information about the last 30 days along with the input, as implemented in the DL models, surpassed other models in performance.

The Hargreaves & Samani model was the best performing empirical model across the seasons, years, and climate divisions, and further performance improvement can be achieved by using the climate division-specific calibration provided in this study. Since CIMIS stations are mainly located in arid/semi-arid regions in California, our models are most reliable and recommended to be used in similar climate conditions. Nevertheless, the study offers a methodology that can be followed in other data-sparse regions. Considering the difficulty in collecting the meteorological input parameters like wind speed and humidity,

Table 6
Performance statistics for the temperature-based ET_o equations and deep learning models for the 15 validation CIMIS stations.

Model	Metric	Mean	std	min	max
BC	RMSE	1.04	0.24	0.75	1.69
	MAE	0.81	0.23	0.54	1.47
	MBE	−0.14	0.57	−1.35	0.67
	NSE	0.75	0.11	0.48	0.89
	R^2	0.75	0.11	0.48	0.89
BC(cal)	RMSE	1.20	0.27	0.92	1.76
	MAE	0.96	0.21	0.75	1.44
	MBE	−0.37	0.55	−1.33	0.36
	NSE	0.68	0.11	0.43	0.83
	R^2	0.68	0.11	0.43	0.83
BC(cal_{cd})	RMSE	1.09	0.16	0.88	1.39
	MAE	0.86	0.12	0.72	1.07
	MBE	−0.27	0.38	−0.87	0.29
	NSE	0.73	0.08	0.62	0.85
	R^2	0.73	0.08	0.62	0.85
HS	RMSE	0.90	0.24	0.53	1.33
	MAE	0.68	0.18	0.38	1.04
	MBE	−0.17	0.42	−0.87	0.47
	NSE	0.81	0.10	0.64	0.94
	R^2	0.81	0.10	0.64	0.94
HS(cal)	RMSE	0.89	0.22	0.53	1.28
	MAE	0.67	0.16	0.38	0.97
	MBE	−0.10	0.42	−0.78	0.54
	NSE	0.82	0.08	0.69	0.94
	R^2	0.82	0.08	0.69	0.94
HS(cal_{cd})	RMSE	0.88	0.22	0.53	1.27
	MAE	0.66	0.15	0.39	0.90
	MBE	−0.12	0.37	−0.66	0.49
	NSE	0.83	0.07	0.72	0.94
	R^2	0.83	0.07	0.72	0.94
ANN_all	RMSE	0.51	0.07	0.39	0.64
	MAE	0.35	0.07	0.27	0.52
	MBE	0.03	0.15	−0.34	0.21
	NSE	0.93	0.04	0.83	0.97
	R^2	0.93	0.04	0.83	0.97
ANN_T	RMSE	0.79	0.20	0.51	1.20
	MAE	0.57	0.16	0.33	0.91
	MBE	−0.14	0.38	−0.70	0.48
	NSE	0.86	0.07	0.74	0.95
	R^2	0.86	0.07	0.74	0.95
LSTM_all	RMSE	0.44	0.08	0.32	0.59
	MAE	0.30	0.05	0.25	0.42
	MBE	0.00	0.11	−0.26	0.16
	NSE	0.95	0.03	0.86	0.98
	R^2	0.95	0.03	0.86	0.98
LSTM_T	RMSE	0.74	0.15	0.58	1.07
	MAE	0.54	0.11	0.38	0.79
	MBE	−0.08	0.34	−0.58	0.51
	NSE	0.87	0.05	0.78	0.93
	R^2	0.87	0.05	0.78	0.93
CNN_all	RMSE	0.47	0.05	0.39	0.58
	MAE	0.35	0.04	0.31	0.45
	MBE	−0.06	0.10	−0.26	0.13
	NSE	0.95	0.03	0.89	0.97
	R^2	0.95	0.03	0.89	0.97
CNN_T	RMSE	0.77	0.16	0.60	1.12
	MAE	0.56	0.12	0.41	0.82
	MBE	−0.03	0.36	−0.55	0.58
	NSE	0.87	0.05	0.78	0.93
	R^2	0.87	0.05	0.78	0.93

(cal) and (cal_{cd}) represents Calibrated and Climate Division specific calibrated models, respectively.

calibrated Hargreaves & Samani, ANN_T, LSTM_T, and CNN_T models that we developed in this study can be adopted for accurate estimations of ET_o across California. Extraterrestrial solar radiation (R_a), another input in the temperature-based models, can be calculated based on location and time of the year following the equations given by Allen et al. (1998). Thus, these models only require on-site air temperature measurements as inputs.

The results of this study and the calibration information can be used for water resource management and irrigation scheduling by irrigation/agricultural experts for reliable ET_o estimations using temperature-based methods. More specifically, DL methods have the potential to be deployed in various smart irrigation controllers that collect on-site temperature information for the estimation of ET_o. The DL models developed in this study can be accessed at http://www.ucrwater.com/software-and-tools.html as a webapp named deepET.

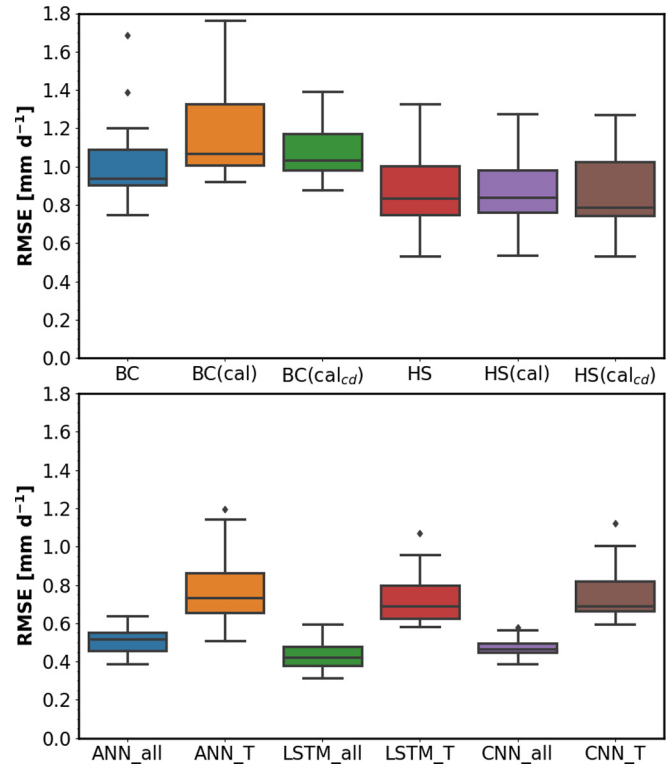

Fig. 10. Boxplot of the root mean squared error (RMSE) observed at 15 validation sites for each model. BC: Blaney & Criddle FAO, HS: Hargreaves & Samani, (cal) and (cal_{cd}) represents Calibrated and Climate Division specific calibrated models, respectively. ANN_all: ANN model with T_{min}, T_{max}, T_a, R_a, RH, and U as inputs, WA-ANN_all: Wavelet transform ANN model with T_{min}, T_{max}, T_a, R_a, RH, and U as inputs, ANN_T: ANN model with T_{min}, T_{max}, T_a, and R_a as inputs, WA-ANN_T: wavelet transform ANN model with T_{min}, T_{max}, T_a, and R_a as inputs, LSTM_all: Long short-Term Memory Recurrent Neural Network with 6 inputs, LSTM_T: 4 inputs, CNN_all: Convolutional neural network with 6 inputs, CNN_T: CNN model with 4 inputs.

CRediT authorship contribution statement

Amninder Singh: Methodology, Formal analysis, Software, Visualization, Data curation, Writing – original draft. **Amir Haghverdi:** Conceptualization, Supervision, Funding acquisition, Writing – review & editing.

Declaration of Competing Interest

The authors declare that they have no known competing financial interests or personal relationships that could have appeared to influence the work reported in this paper.

References

Adamala, S., 2018. Temperature based generalized wavelet-neural network models to estimate evapotranspiration in India. Inform. Process. Agric. 5, 149–155. https://doi.org/10.1016/j.inpa.2017.09.004.
Adamowski, J., Sun, K., 2010. Development of a coupled wavelet transform and neural network method for flow forecasting of non-perennial rivers in semi-arid watersheds. J. Hydrol. (Amst.) 390, 85–91. https://doi.org/10.1016/j.jhydrol.2010.06.033.
Alexandridis, A.K., Zapranis, A.D., 2013. Wavelet neural networks: a practical guide. Neural Netw. 42, 1–27. https://doi.org/10.1016/j.neunet.2013.01.008.
Allen, R.G., Pruitt, W.O., 1986. Rational use of the FAO Blaney-Criddle formula. J. Irrig. Drain. Eng. 112, 139–155.

Allen, R.G., Pruitt, W.O., 1991. FAO-24 reference evapotranspiration factors. J. Irrig. Drain. Eng. 117, 758–773.
Allen, R.G., Pereira, L.S., Raes, D., Smith, M., 1998. Crop Evapotranspiration FAO Irrigation and Drainage Paper No. 56.
Allen, R.G., Walter, I.A., Elliott, R.L., Howell, T.A., Itenfisu, D., Jensen, M.E., Snyder, R.L., 2005. The ASCE Standardized Reference Evapotranspiration Equation. Technical Committee on Standardization of Reference Evapotranspiration, Books. American Society of Civil Engineers, Reston, VA. https://doi.org/10.1061/9780784408056.
Cardenas, B., Dukes, M.D., Breder, E., Torbert, J.W., 2021. Long-term performance of smart irrigation controllers on single-family homes with excess irrigation. AWWA Water Sci. 3, 1–14. https://doi.org/10.1002/aws2.1218.
Chen, Z., Zhu, Z., Jiang, H., Sun, S., 2020. Estimating daily reference evapotranspiration based on limited meteorological data using deep learning and classical machine learning methods. J. Hydrol. (Amst.) 591, 125286. https://doi.org/10.1016/j.jhydrol.2020.125286.
Cobaner, M., 2013. Reference evapotranspiration based on class A pan evaporation via wavelet regression technique. Irrig. Sci. 31, 119–134. https://doi.org/10.1007/s00271-011-0297-x.
Davis, S.L., Dukes, M.D., 2010. Irrigation scheduling performance by evapotranspiration-based controllers. Agric. Water Manag. 98, 19–28. https://doi.org/10.1016/j.agwat.2010.07.006.
Djaman, K., Balde, A.B., Sow, A., Muller, B., Irmak, S., N'Diaye, M.K., Manneh, B., Moukoumbi, Y.D., Futakuchi, K., Saito, K., 2015. Evaluation of sixteen reference evapotranspiration methods under sahelian conditions in the Senegal River valley. J. Hydrol. Reg. Stud. 3, 139–159. https://doi.org/10.1016/j.ejrh.2015.02.002.
Donald Frevert, B.K., Asce, M., Hill, R.W., Braaten, B.C., Members ASCE A, 1983. Estimation of FAO evapotranspiration coefficients. J. Irrig. Drain. Eng. 109, 265–270. https://doi.org/10.1061/(ASCE)0733-9437(1983)109:2(265).
Doorenbos, J., Pruitt, W.O., 1977. Guidelines for predicting crop water requirements. FAO Irrigat. Drain. Pap. 24, 144.
Elbeltagi, A., Deng, J., Wang, K., Malik, A., Maroufpoor, S., 2020. Modeling long-term dynamics of crop evapotranspiration using deep learning in a semi-arid environment. Agric. Water Manag. 241, 106334. https://doi.org/10.1016/j.agwat.2020.106334.
Evrendilek, F., 2014. Assessing neural networks with wavelet denoising and regression models in predicting diel dynamics of eddy covariance-measured latent and sensible heat fluxes and evapotranspiration. Neural Comput. & Applic. 24, 327–337. https://doi.org/10.1007/s00521-012-1240-7.
Falamarzi, Y., Palizdan, N., Huang, Y.F., Lee, T.S., 2014. Estimating evapotranspiration from temperature and wind speed data using artificial and wavelet neural networks (WNNs). Agric. Water Manag. 140, 26–36. https://doi.org/10.1016/j.agwat.2014.03.014.
Fan, J., Yue, W., Wu, L., Zhang, F., Cai, H., Wang, X., Lu, X., Xiang, Y., 2018. Evaluation of SVM, ELM and four tree-based ensemble models for predicting daily reference evapotranspiration using limited meteorological data in different climates of China. Agric. For. Meteorol. 263, 225–241. https://doi.org/10.1016/j.agrformet.2018.08.019.
Ferreira, L.B., da Cunha, F.F., 2020. New approach to estimate daily reference evapotranspiration based on hourly temperature and relative humidity using machine learning and deep learning. Agric. Water Manag. 234, 106113. https://doi.org/10.1016/j.agwat.2020.106113.
Gabriela Arellano, M., Irmak, S., 2016. Reference (potential) evapotranspiration. I: comparison of temperature, radiation, and combination-based energy balance equations in humid, subhumid, arid, semiarid, and Mediterranean-type climates. J. Irrig. Drain. Eng. 142, 04015065. https://doi.org/10.1061/(ASCE)IR.1943-4774.0000978.
Haghverdi, A., Reiter, M., Sapkota, A., Singh, A., 2021a. Hybrid Bermudagrass and tall fescue Turfgrass irrigation in Central California: I. assessment of visual quality, soil moisture and performance of an ET-based smart controller. Agronomy 11, 1666. https://doi.org/10.3390/agronomy11081666.
Haghverdi, A., Singh, A., Sapkota, A., Reiter, M., Ghodsi, S., 2021b. Developing irrigation water conservation strategies for hybrid bermudagrass using an evapotranspiration-based smart irrigation controller in inland southern California. Agric. Water Manag. 245, 106586. https://doi.org/10.1016/j.agwat.2020.106586.
Han, Z., Zhao, J., Leung, H., Ma, K.F., Wang, W., 2021. A review of deep learning models for time series prediction. IEEE Sensors J. 21, 7833–7848. https://doi.org/10.1109/JSEN.2019.2923982.
Hargreaves, G.H., Allen, R.G., 2003. History and evaluation of Hargreaves evapotranspiration equation. J. Irrig. Drain. Eng. 129, 53–63. https://doi.org/10.1061/(ASCE)0733-9437(2003)129:1(53).
Hargreaves, G.H., Samani, Z.A., 1985. Reference crop evapotranspiration from temperature. Appl. Eng. Agric. 1, 96–99. https://doi.org/10.13031/2013.26773.
Hidalgo, H.G., Cayan, D.R., Dettinger, M.D., 2005. Sources of variability of evapotranspiration in California. J. Hydrometeorol. 6, 3–19. https://doi.org/10.1175/JHM-398.1.
Hochreiter, S., Schmidhuber, J., 1997. Long short-term memory. Neural Comput. 9, 1735–1780. https://doi.org/10.1162/NECO.1997.9.8.1735.
Hope, A.S., Evans, S.M., 1993. Estimating reference evaporation in the Central Valley of California using the Linacre model. Water Resour. Bull. Am. Water Resour. Assoc. 28, 695–702.
Kingma, D.P., Ba, J.L., 2015. Adam: A Method for Stochastic Optimization, in: 3rd International Conference on Learning Representations, ICLR 2015 - Conference Track Proceedings. International Conference on Learning Representations, ICLR.
Kişi, Ö., 2010. Evapotranspiration modeling using a wavelet regression model. Irrig. Sci. https://doi.org/10.1007/s00271-010-0232-6.
Kisi, O., Alizamir, M., 2018. Modelling reference evapotranspiration using a new wavelet conjunction heuristic method: wavelet extreme learning machine vs wavelet neural networks. Agric. For. Meteorol. 263, 41–48. https://doi.org/10.1016/j.agrformet.2018.08.007.
Kukal, M., Irmak, S., Walia, H., Odhiambo, L., 2020. Spatio-temporal calibration of Hargreaves-Samani model to estimate reference evapotranspiration across U.S. High Plains. Agron. J., 1–17. https://doi.org/10.1002/agj2.20325.
Lee, G., Gommers, R., Waselewski, F., Wohlfahrt, K., O'Leary, A., 2019. PyWavelets: a Python package for wavelet analysis. J. Open Source Softw. 4, 1237. https://doi.org/10.21105/joss.01237.
Li, D., Zhang, J., Zhang, Q., Wei, X., 2017. Classification of ECG signals based on 1D convolution neural network. 2017 IEEE 19th International Conference on E-Health Networking, Applications and Services, Healthcom 2017. Institute of Electrical and Electronics Engineers Inc., pp. 1–6. https://doi.org/10.1109/HealthCom.2017.8210784.
Liu, X., Xu, C., Zhong, X., Li, Y., Yuan, X., Cao, J., 2017. Comparison of 16 models for reference crop evapotranspiration against weighing lysimeter measurement. Agric. Water Manag. 184, 145–155. https://doi.org/10.1016/j.agwat.2017.01.017.
Long, H., Shuai, X., Lei, Q., Zhang, R., 2013. Spatiotemporal distribution of calibration coefficients of Hargreaves equation for estimating potential evapotranspiration in mainland China. J. Irrig. Drain. Eng. 139, 293–299. https://doi.org/10.1061/(asce)ir.1943-4774.0000534.
Long, X., Wang, J., Gong, S., Li, G., Ju, H., 2022. Reference evapotranspiration estimation using long short-term memory network and wavelet-coupled long short-term memory network. Irrig. Drain. https://doi.org/10.1002/ird.2699.
Muhammad, M.K.I., Nashwan, M.S., Shahid, S., Ismail, T., Song, Y.H., Chung, E.S., 2019. Evaluation of empirical reference evapotranspiration models using compromise programming: a case study of peninsular Malaysia. Sustainability (Switzerland) 11. https://doi.org/10.3390/su11164267.
Muniandy, J.M., Yusop, Z., Askari, M., 2016. Evaluation of reference evapotranspiration models and determination of crop coefficient for Momordica charantia and Capsicum annuum. Agric. Water Manag. 169, 77–89. https://doi.org/10.1016/j.agwat.2016.02.019.
Partal, T., 2009. Modelling evapotranspiration using discrete wavelet transform and neural networks. Hydrol. Process. 23, 3545–3555. https://doi.org/10.1002/hyp.7448.
Pruitt, W.O., Doorenbos, J., 1977. Empirical calibration, a requisite for evapotranspiration formulae based on daily or longer mean climate data. Int. Comm. on Irrig. and Drain., Budapest, Hungary, p. 20.
Saggi, M.K., Jain, S., 2019. Reference evapotranspiration estimation and modeling of the Punjab northern India using deep learning. Comput. Electron. Agric. 156, 387–398. https://doi.org/10.1016/j.compag.2018.11.031.
Senatore, A., Parrello, C., Almorox, Javier, Mendicino, G., 2020. Exploring the potential of temperature-based methods for regionalization of daily reference evapotranspiration in two Spanish regions. J. Irrig. Drain. Eng. 146, 05020001. https://doi.org/10.1061/(ASCE)IR.1943-4774.0001447.
Serena, M., Velasco-Cruz, C., Friell, J., Schiavon, M., Sevostianova, E., Beck, L., Sallenave, R., Leinauer, B., 2020. Irrigation scheduling technologies reduce water use and maintain turfgrass quality. Agron. J. 112, 3456–3469. https://doi.org/10.1002/agj2.20246.
Sharma, G., Singh, A., Jain, S., 2022. A hybrid deep neural network approach to estimate reference evapotranspiration using limited climate data. Neural Comput. & Applic. 34, 4013–4032. https://doi.org/10.1007/s00521-021-06661-9.
Sowmya, M.R., Santosh Kumar, M.B., Ambat, S.K., 2020. Comparison of deep neural networks for reference evapotranspiration prediction using minimal meteorological data. Proceedings - 2020 Advanced Computing and Communication Technologies for High Performance Applications, ACCTHPA 2020. Institute of Electrical and Electronics Engineers Inc., pp. 27–33 https://doi.org/10.1109/ACCTHPA49271.2020.9213201.
Tabari, H., Grismer, M.E., Trajkovic, S., 2013. Comparative analysis of 31 reference evapotranspiration methods under humid conditions. Irrig. Sci. 31, 107–117. https://doi.org/10.1007/s00271-011-0295-z.
Temesgen, B., Allen, R.G., Jensen, D.T., 1999. Adjusting temperature parameters to reflect well-watered conditions. J. Irrig. Drain. Eng. 125, 26–33. https://doi.org/10.1061/(ASCE)0733-9437(1999)125:1(26).
Temesgen, B., Eching, S., Davidoff, B., Frame, K., 2005. Comparison of some reference evapotranspiration equations for California. J. Irrig. Drain. Eng. 131, 73–84. https://doi.org/10.1061/(ASCE)0733-9437(2005)131:1(73).
TensorFlow Developers, 2021. TensorFlow. https://doi.org/10.5281/ZENODO.5189249.
Trabucco, A., Zomer, R.J., 2018. Global Aridity Index and Potential Evapo-Transpiration (ET0) Climate Database v2. CGIAR Consortium for Spatial Information (CGIAR-CSI) Published online, available from the CGIAR-CSI GeoPortal at https://cgiarcsi.community.
Traore, S., Wang, Y.M., Kerh, T., 2010. Artificial neural network for modeling reference evapotranspiration complex process in Sudano-Sahelian zone. Agric. Water Manag. 97, 707–714. https://doi.org/10.1016/j.agwat.2010.01.002.
Traore, S., Luo, Y., Fipps, G., 2016. Deployment of artificial neural network for short-term forecasting of evapotranspiration using public weather forecast restricted messages. Agric. Water Manag. 163, 363–379. https://doi.org/10.1016/j.agwat.2015.10.009.
Xu, C.-Y., Singh, V.P., 2001. Evaluation and generalization of temperature-based methods for calculating evaporation. Hydrol. Process. 15, 305–319. https://doi.org/10.1002/hyp.119.
Yao, Y., Rosasco, L., Caponnetto, A., 2007. On early stopping in gradient descent learning. Constr. Approx. 26 (2), 289–315. https://doi.org/10.1007/S00365-006-0663-2.
Yin, J., Deng, Z., Ines, A.V.M., Wu, J., Rasu, E., 2020. Forecast of short-term daily reference evapotranspiration under limited meteorological variables using a hybrid bi-directional long short-term memory model (bi-LSTM). Agric. Water Manag. 242, 106386. https://doi.org/10.1016/J.AGWAT.2020.106386.
Zhang, Q., Benveniste, A., 1992. Wavelet networks. IEEE Trans. Neural Netw. 3, 889–898. https://doi.org/10.1109/72.165591.